Cell Reports

Article

MCT1 Deletion in Oligodendrocyte Lineage Cells Causes Late-Onset Hypomyelination and Axonal Degeneration

Graphical Abstract

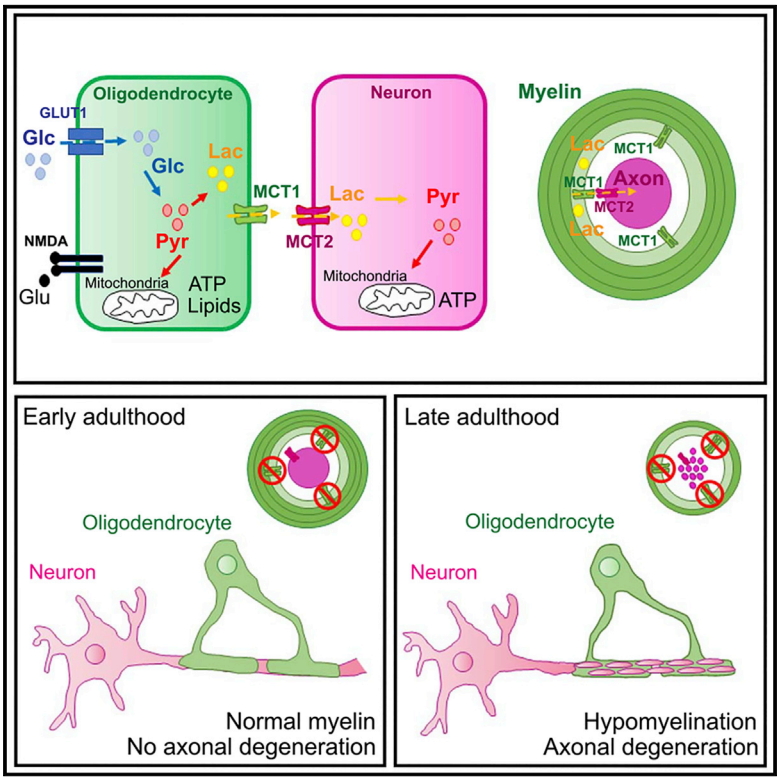

Highlights

- Lack of MCT1-mediated oligodendrocyte metabolic support is well tolerated early on
- Loss of oligodendrocyte MCT1-driven metabolic support causes axonal degeneration
- Loss of oligodendrocyte MCT1-mediated metabolic support causes axonal hypomyelination

Authors

Thomas Philips, Yevgeniya A. Mironova, Yan Jouroukhin, ..., Dwight E. Bergles, Brett M. Morrison, Jeffrey D. Rothstein

Correspondence

bmorris7@jhmi.edu (B.M.M.), jrothstein@jhmi.edu (J.D.R.)

In Brief

Using conditional cell-specific deletion of MCT1, Philips et al. learn that oligodendrocyte lineage cells are actually dispensable for normal myelination and axonal energy homeostasis during early life but that the oligodendroglial lactate/MCT1-based support is critical for the aging of the nervous system.

Philips et al., 2021, Cell Reports *34*, 108610
January 12, 2021
https://doi.org/10.1016/j.celrep.2020.108610

CellPress

Cell Reports

CellPress
OPEN ACCESS

Article

MCT1 Deletion in Oligodendrocyte Lineage Cells Causes Late-Onset Hypomyelination and Axonal Degeneration

Thomas Philips,[1,2] Yevgeniya A. Mironova,[3] Yan Jouroukhin,[4] Jeannie Chew,[1,2] Svetlana Vidensky,[1,2] Mohamed H. Farah,[1] Mikhail V. Pletnikov,[5] Dwight E. Bergles,[3,6] Brett M. Morrison,[1,2,*] and Jeffrey D. Rothstein[1,2,3,7,*]

[1]Department of Neurology, Johns Hopkins University School of Medicine, Baltimore, MD 21205, USA
[2]Brain Science Institute, Johns Hopkins University School of Medicine, Baltimore, MD 21205, USA
[3]Solomon H. Snyder Department of Neuroscience, Johns Hopkins University School of Medicine, Baltimore, MD 21205, USA
[4]Department of Psychiatry and Behavioral Sciences, Johns Hopkins University School of Medicine, Baltimore, MD 21205, USA
[5]Department of Physiology and Biophysics, Jacobs School of Medicine and Biomedical Sciences SUNY, University at Buffalo, Buffalo, NY 14203, USA
[6]Kavli Neuroscience Discovery Institute, Johns Hopkins University, Baltimore, MD 21205, USA
[7]Lead Contact
*Correspondence: bmorris7@jhmi.edu (B.M.M.), jrothstein@jhmi.edu (J.D.R.)
https://doi.org/10.1016/j.celrep.2020.108610

SUMMARY

Oligodendrocytes (OLs) are important for myelination and shuttling energy metabolites lactate and pyruvate toward axons through their expression of monocarboxylate transporter 1 (MCT1). Recent studies suggest that loss of OL MCT1 causes axonal degeneration. However, it is unknown how widespread and chronic loss of MCT1 in OLs specifically affects neuronal energy homeostasis with aging. To answer this, MCT1 conditional null mice were generated that allow for OL-specific MCT1 ablation. We observe that MCT1 loss from OL lineage cells is dispensable for normal myelination and axonal energy homeostasis early in life. By contrast, loss of OL lineage MCT1 expression with aging leads to significant axonal degeneration with concomitant hypomyelination. These data support the hypothesis that MCT1 is important for neuronal energy homeostasis in the aging central nervous system (CNS). The reduction in OL MCT1 that occurs with aging may enhance the risk for axonal degeneration and atrophy in neurodegenerative diseases.

INTRODUCTION

In the central nervous system (CNS), the capacity of neurons to provide for their own energy homeostasis is insufficient and highly dependent on metabolic and trophic support from glial cells (Saab and Nave, 2017; Magistretti and Allaman, 2018; Alberini et al., 2018; Argente-Arizón et al., 2017). Oligodendrocytes (OLs), which are myelin-generating cells, play a key role in glial-axonal signaling and metabolic support to neurons (Griffiths et al., 1998; Lappe-Siefke et al., 2003; Brady et al., 1999; Yin et al., 1998). Among the metabolites that mediate this OL energy support function are the monocarboxylates lactate and pyruvate (Lee et al., 2012; Fünfschilling et al., 2012). OLs appear to generate lactate and pyruvate in an activity-dependent manner: glutamate release from neurons activates NMDA receptors on OLs, increasing glucose uptake and lactate production through glycolysis (Saab et al., 2016). In order to prevent lactate accumulation, acidosis, and cell death, OLs shuttle lactate into the extracellular space through monocarboxylate transporters. Along with other glial and endothelial cells, OLs express monocarboxylate transporter 1 (MCT1, Slc16a1) that passively transports lactate and hydrogen toward the intra- or extracellular space, depending on the substrate concentration gradient across the plasma membrane (Lee et al., 2012; Rinholm et al., 2011). From the extracellular space, neurons can take up lactate through MCT1 and monocarboxylate transporter 2 (MCT2) and use lactate to fuel energy demands (Pierre et al., 2000; Rinholm et al., 2011). Prior studies have highlighted the importance of MCT1 in providing neurons with trophic support (Lee et al., 2012). Mice with only one genetic copy of *Mct1* develop axonal degeneration by 8 months of age. Moreover, focal lentiviral vector-mediated knockdown of *Mct1* specifically in OLs causes axonal injury, suggesting that the phenotype observed in *Mct1* heterozygous (het) mice is, in part, mediated by a reduction in MCT1 expression by OLs. As loss of OL MCT1 expression has also been observed in human neurodegenerative disease and animal models of these diseases (Lee et al., 2012; Philips et al., 2013; Tang et al., 2019; Andres Benito et al., 2018), it could severely affect neuronal function and contribute to neuronal degeneration.

In this study, we test the prevailing hypothesis that OL MCT1 is required for axonal survival. In addition, the contribution of aging, in which neuronal energy homeostasis is altered (Mattson and Magnus, 2006), to the maintenance of OL-dependent neuronal

function through OL MCT1 is evaluated. Our previous study focused on the pathological consequences of either ubiquitous knockdown of MCT1 in *Slc16a1* het mice or the effects of focal knockdown of OL MCT1 on the surrounding axons, but essential questions still remain unanswered (Lee et al., 2012). First, MCT1 is expressed by multiple cells types including astrocytes and endothelial cells; therefore, the specific contribution of OL MCT1 metabolic support is impossible to extrapolate from the studies using *Mct1* het mice. Second, focal knockdown of OL MCT1 by injection of lentivirus-encoding small hairpin RNAs (shRNAs) targeting MCT1 causes local tissue damage and inflammation that may impact axon degeneration. And third, the past lentiviral studies do not provide information on the long-term consequences of OL MCT1 loss throughout the entire CNS. To address these issues, we generated a conditional MCT1 mouse line (Jha et al., 2020) that we used to knock out MCT1 either specifically in mature OLs or across the entire OL lineage. These two approaches allow us to examine the consequences of MCT1 loss at various stages of OL development, including OL precursor cells (OPCs), differentiating OLs, and mature OLs, on both OL myelination and neuronal metabolic support throughout the animal's lifespan.

RESULTS

OL MCT1 Expression Is Significantly Reduced with Aging

We first evaluated whether OL MCT1 expression undergoes dynamic changes with aging that could impact neuronal energy demands. To test *Mct1* mRNA expression in OLs, we used *Mct1-tdTomato* mice, which express tdTomato (tdT) under control of the *Mct1* promoter (Lee et al., 2012). To assess promoter activity in OLs over time, immunofluorescence co-localization studies were performed for tdT and the mature OL marker adenomatous polyposis coli clone (CC1) in lumbar gray matter spinal cord, at ages ranging from post-natal day 60 (P60) to P550. Aging had no effect on the percentage of tdT^+ OLs in the spinal cord of *Mct1-tdTomato* mice (Figure 1A). Subsequently, MCT1 promoter activity during OL maturation was evaluated using *Mct1-tdTomato* mice crossed with *Pdgfrα-CreER* and *RosaYFP* reporter mice. These triple-transgenic animals were injected intraperitoneally with tamoxifen at different ages (P60, P200, P360, and P500) to induce yellow fluorescent protein (YFP) labeling of OPCs. Thirty days after the first tamoxifen injection, YFP-labeled OPCs that differentiated into tdT^+CC1^+-expressing OLs were quantified in the lumbar spinal cord gray matter. Despite the significant decrease in oligodendrogenesis within the YFP-labeled cell pool with aging (fraction $CC1^+YFP^+/YFP^+$ cells: 54% by P230 and 80% by P530), the ability of newly generated $CC1^+YFP^+$ OLs to express tdT was unaffected (fraction $CC1^+YFP^+MCT1tdT^+/CC1^+YFP^+$; Figures 1B–1D), suggesting that these newly generated OLs maintain *Mct1* promoter activity. Dynamic changes in OL MCT1 protein with aging were evaluated in purified myelin protein extracts derived from the spinal cord of aged animals. Interestingly, unlike for the *Mct1* promoter activity, spinal cord myelin MCT1 protein expression had declined by 35% by the age of P360, when mice are considered middle age, corresponding to age 38–47 years in humans (Flurkey et al., 2007) (Figure 1E). These data suggest that OLs gradually lose their ability to provide monocarboxylates to neurons. These observations are in line with earlier reported changes in neuronal integrity, energy homeostasis, and autophagic flux that occur with normal aging in mouse and human CNS (Stavoe and Holzbaur, 2019; Mattson and Magnus, 2006; Salvadores et al., 2017).

Conditional Loss of MCT1 in the OL Lineage Cells Significantly Affects MCT1 Expression and Transporter Activity

Mct1 conditional null mice were generated in our laboratory by transgenic insertion of loxP sites flanking exon 2 of the *Mct1* gene (Jha et al., 2020). To target *Mct1* specifically in OL lineage cells, two approaches were followed. The conditional *Mct1* null mice ($MCT1^{lox}$) were crossed with either the mature OL-specific Cre line *MogCre* (Mog^{Cre}) or with the pan-OL lineage Cre mouse line *Sox10Cre* ($Sox10^{Cre}$) to generate either $Sox10^{Cre}$-$MCT1^{lox}$ or Mog^{Cre}-$MCT1^{lox}$ mice, respectively, hemizygous for Cre and homozygous for $MCT1^{lox}$. Homozygous age-matched $MCT1^{lox}$ mice were used as littermate controls throughout all experiments. $Sox10^{Cre}$ mice were used to evaluate the importance of MCT1 during differentiation and myelination in addition to its function in mature OLs. Mog^{Cre} mice were used to determine the role of MCT1 in mature OLs specifically.

Efficacy of MCT1 conditional ablation was measured at RNA and protein level in whole-tissue CNS lysates prepared from either P45 Mog^{Cre}-$MCT1^{lox}$ or Sox^{Cre}-$MCT1^{lox}$ mice and their $MCT1^{lox}$ littermate controls. In spinal cord and cortex, modest reductions were observed for MCT1 protein (Figures 2A and 2B), which likely reflect MCT1 expression in other cell types such as astrocytes and endothelial cells as we confirmed by immunostaining (Figure S1B). Whereas *Mct1* mRNA was only modestly affected in the Mog^{Cre}-$MCT1^{lox}$ mice (Figure S1A), $Sox10^{Cre}$-$MCT1^{lox}$ mice had a 51% reduction of *Mct1* mRNA expression in the spinal cord and a 38% reduction in the cortex compared with $MCT1^{lox}$ controls (Figure 2C). This is a far greater effect compared with loss of *Mct1* mRNA in spinal cord (24%) and cortex (12%) in the astrocyte conditional MCT1 null mice (unpublished data). In addition, $O4^+$ OL lineage cells isolated from the cortex of P150 $Sox10^{Cre}$-$MCT1^{lox}$ mice have 76% reduction in *Mct1* mRNA compared with $MCT1^{lox}$ controls (Figure 2C). To enrich for OL-specific MCT1 protein, myelin fractions were biochemically fractionated and purified from cortex and spinal cord. In P30 Mog^{Cre}-$MCT1^{lox}$ mice, MCT1 expression in myelin fractions derived from spinal cord was reduced by 81%, whereas cortical myelin MCT1 expression was reduced by 40% at P30 and 80% at P180. (Figure 2D; Figure S1C). In myelin fractions derived from P30 $Sox10^{Cre}$-$MCT1^{lox}$ mice, MCT1 protein expression was reduced by 84% in spinal cord and 81% in cortex (Figure 2E). Lastly, MCT1 transporter activity was measured in primary cultures of OPCs/OLs generated from cortices of P7-old $Sox10^{Cre}$-$MCT1^{lox}$ and $MCT1^{lox}$ mice. Radioactive [^{14}C]lactate uptake in cultures obtained from $Sox10^{Cre}$-$MCT1^{lox}$ mice was reduced by 75% compared with $MCT1^{lox}$ controls, comparable to the uptake obtained when treating the $MCT1^{lox}$ OL lineage cultures with 1 μM MCT1 inhibitor AR-C155858 (Figure 2F). The uptake of radioactive [^{14}C]pyruvate revealed a 68% reduction in [^{14}C]pyruvate uptake in the

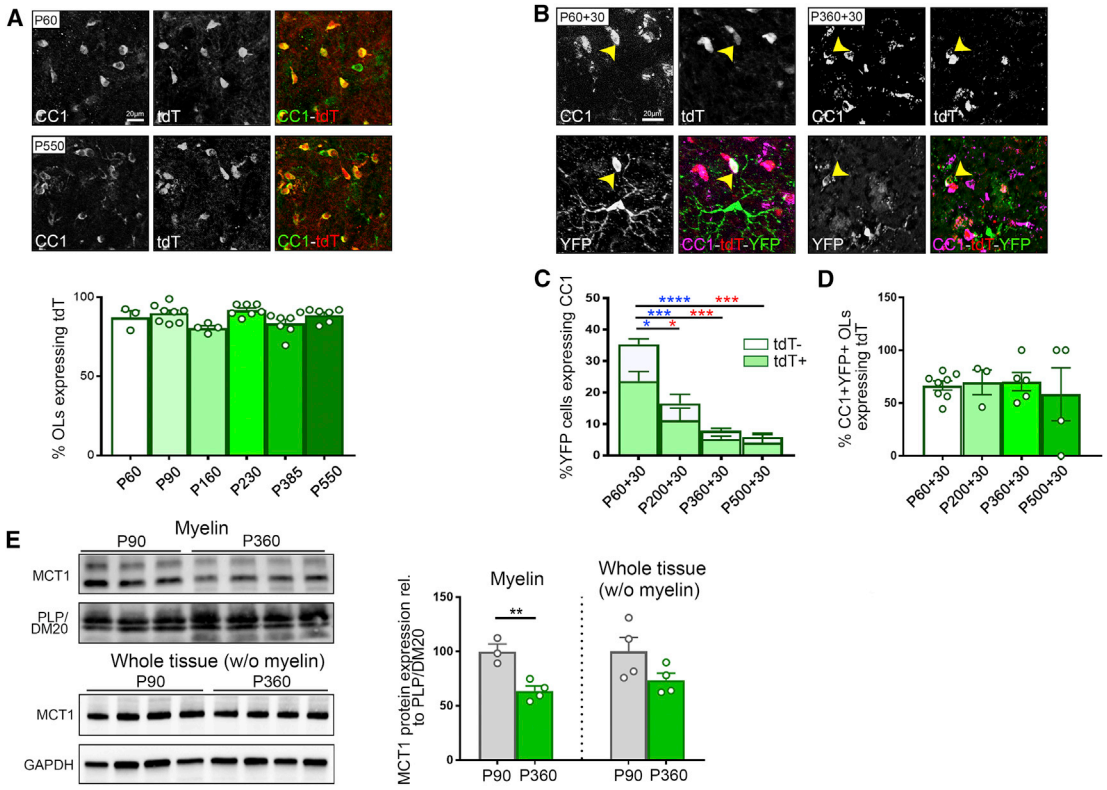

Figure 1. Loss of Oligodendrocyte (OL) MCT1 Protein Expression with Aging

(A) Immunostaining and quantification of CC1$^+$ OLs expressing MCT1-tdTomato (tdT) between the ages of P60 and P550 (n = 3–8). Data are represented as mean ± SEM.

(B) Evaluation of the ability of newly generated OLs to express tdT. P60-, P200-, P360-, and P550-old *Pdgfrα-CreER-RosaYFP-MCT1td-Tomato* mice were injected with tamoxifen to induce YFP labeling of OPCs and were euthanized 30 days later. Immunostaining highlights differentiated CC1$^+$ OLs expressing tdT and YFP at the ages of P60+30 and P360+30. Images are representative of n = 5–8.

(C and D) Quantification of the fraction of newly generated OLs (# CC1$^+$YFP$^+$/# YFP$^+$, full bars, statistics in blue) and the fraction of newly generated OLs expressing tdT (# CC1$^+$YFP$^+$MCT1tdTomato$^+$/# YFP$^+$, light green bars, statistics in red) reveals a significant decrease with aging (C) (n = 4–8, *p < 0.05, ***p < 0.001, ****p < 0.0001, one-way ANOVA with Tukey's multiple comparison test). The fraction of newly differentiated OLs that turn on tdT expression (# CC1$^+$YFP$^+$MCT1tdTomato$^+$/# CC1$^+$YFP$^+$) is unaffected by aging (D) (n = 3–8). Data are represented as mean ± SEM.

(E) Western blot analysis of MCT1 protein in purified myelin fractions reveals a 35% reduction at P360 compared with P90 (n = 3-4, **p < 0.01, Student's t test), whereas MCT1 protein expression in the "whole tissue (without [w/o] myelin)" fraction is unchanged. Data are represented as mean ± SEM.

Sox10^{Cre}-MCT1^{lox} cultures compared with MCT1^{lox} controls (Figure 2F). In summary, these data indicate that our conditional knockout approach results in loss of MCT1 function in the OL lineage.

Conditional Loss of MCT1 in OLs Has Subtle Effects on the mRNA, but Not Protein, Expression of Other MCTs and Connexin Hemichannels

Apart from MCTs, glial cells express glucose transporters and connexin hemichannels that allow for the transport of energy metabolites across plasma membranes. Loss of MCT1 expression in OL lineage cells could be compensated by increased expression of MCTs MCT2 and MCT4, glucose transporter 1 (GLUT1) and GLUT3, or connexin hemichannels (OL: *Gjc2* (Cx47); astrocytes: *Gja1* (Cx43) and *Gjb6* (Cx30)). Spinal cord mRNA and protein extracts isolated from P45-old Mog^{Cre}-MCT1^{lox} mice and MCT1^{lox} controls were evaluated for changes in transporter or connexin hemichannel expression. A 1.3- and 1.2-fold increase in the expression of *Mct2* and *Mct4* mRNA was observed in the spinal cord of Mog^{Cre}-MCT1^{lox} mice and a 1.3-fold increase in astrocyte connexin *Cx43* mRNA and OL connexin *Cx47* mRNA (Figures 3A and 3B). Protein analysis did not reveal significant changes in MCT2 or Cx43 protein, and MCT4 expression was undetectable by western blotting (Figures 3D and 3E; data not shown). There were no changes in GLUT1 and GLUT3 expression at either mRNA or protein level (Figures 3C and 3F). In addition, no significant changes were observed in *Glut*, connexin, and *Mct2/4* mRNA expression in spinal cord tissue derived from Sox10^{Cre}-MCT1^{lox} and MCT1^{lox} mice (Figures 3G–3I). In summary, these data suggest that neither Sox10^{Cre}- nor Mog^{Cre}-mediated depletion of MCT1 has a strong impact on the expression of other metabolic transporters. We did observe a subtle upregulation in *Cx43* and *Cx47* hemichannel and *Mct2/4* mRNA expression in the Mog^{Cre} conditional nulls, but not in the Sox10^{Cre} conditional nulls, which could underlie a metabolic compensation for the loss of MCT1.

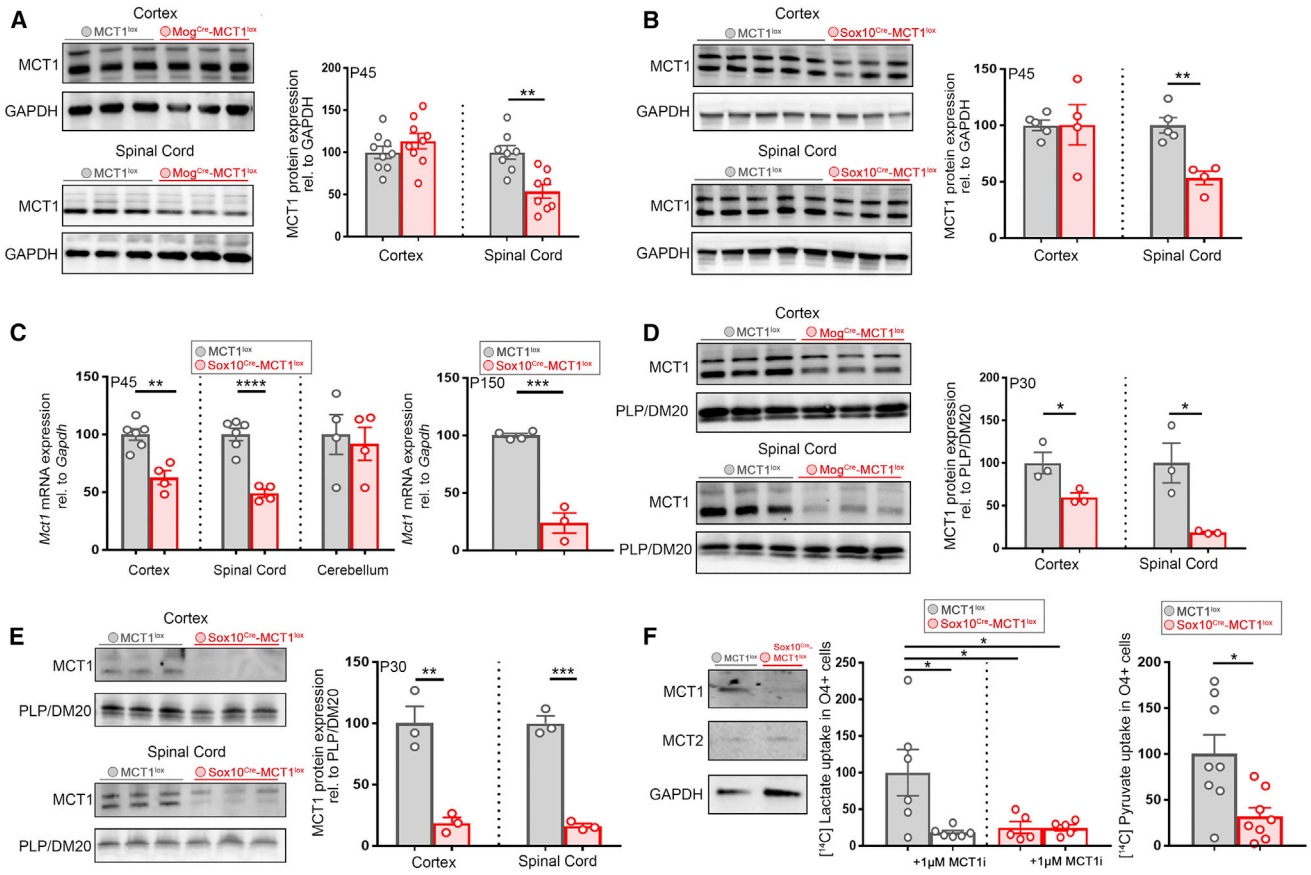

Figure 2. Loss of MCT1 Protein and Transporter Activity in the Mog^{Cre}-MCT1^{lox} and Sox10^{Cre}-MCT1^{lox} Conditional Null Mice

(A) MCT1 expression in whole spinal cord tissue lysates from P45 Mog^{Cre}-MCT1^{lox} mice is reduced by 46% compared with MCT1^{lox} controls, whereas the cortical MCT1 expression is unchanged (n = 8–9, **p < 0.01, Student's t test). Data are represented as mean ± SEM.

(B) MCT1 protein expression in whole-tissue lysates from spinal cord derived from P45 Sox10^{Cre}-MCT1^{lox} and MCT1^{lox} controls is reduced by 47% in the conditional nulls, whereas cortical MCT1 protein expression is unchanged (n = 4–5, **p < 0.01, Student's t test). Data are represented as mean ± SEM.

(C) Left: *Mct1* exon 2 mRNA expression analysis in P45 Sox10^{Cre}-MCT1^{lox} and MCT1 ^{lox} mice whole CNS tissue RNA extracts is reduced by 51% in spinal cord and 37% in the cortex (Ctx) of the conditional nulls, whereas cerebellar *Mct1* mRNA expression is unchanged (n = 4–6, **p < 0.01 and ****p < 0.0001, Student's t test). Right: *Mct1* mRNA expression in cortical O4^{+} progenitors isolated from P150 MCT1^{lox} and Sox10^{Cre}-MCT1^{lox} mice is reduced by 76% in the conditional nulls (n = 3–4, ***p < 0.001, Student's t test). Data are represented as mean ± SEM.

(D) MCT1 protein in myelin fractions derived from Ctx and spinal cord of P30 Mog^{Cre}-MCT1^{lox} mice and MCT1^{lox} mice is reduced by 40% in the Ctx and 81% in the spinal cord of the conditional nulls (n = 3, *p < 0.05, Student's t test). Data are represented as mean ± SEM.

(E) Quantification of MCT1 protein expression in myelin fractions derived from spinal cord and Ctx from P30 Sox10^{Cre}-MCT1^{lox} and MCT1 ^{lox} mice reveals an 84% reduction in the spinal cord and an 81% reduction in the Ctx of the conditional null mice (n = 3, ***p < 0.001, **p < 0.01, Student's t test). Data are represented as mean ± SEM.

(F) MCT protein expression in OL lineage cultures derived from Sox10^{Cre}-MCT1^{lox} and MCT1^{lox} P3 pups. MCT1 expression is absent from O4^{+} progenitor cell cultures derived from Sox10^{Cre}-MCT1^{lox} pups and is not compensated by changes in MCT2 expression. Quantification of [^{14}C]lactate uptake in OL lineage cultures reveals a 75% reduction in the Sox10^{Cre}-MCT1^{lox}-derived cultures compared with the MCT1^{lox}-cultured cells. Treatment with 1 μM MCT1 inhibitor AR-C155858 (MCT1i) affects [^{14}C]lactate uptake in MCT1^{lox} cultures by 82% (n = 5–6, *p < 0.05, one-way ANOVA with Tukey's multiple comparison test). Quantification of [^{14}C]pyruvate uptake between Sox10^{Cre}-MCT1^{lox} and MCT1^{lox} OL lineage cultures reveals a 68% reduction in [^{14}C]pyruvate uptake in the conditional nulls (n = 8, *p < 0.05, Student's t test). Data are represented as mean ± SEM.

OL MCT1 Null Mice Develop Normally through Early Adulthood

If OL MCT1 is essential for providing metabolic support to neurons, we expect that loss of MCT1 would impact animal behavior, including locomotion and cognition. P90 Sox10^{Cre}-MCT1^{lox} mice and age-matched MCT1^{lox} littermates were examined for behavioral changes related to general locomotor activity, anxiety, and long-term memory consolidation (summarized in Table S1). The motor performance and exploratory behavior of Sox10^{Cre}-MCT1^{lox} mice were indistinguishable from those of MCT1^{lox} littermate controls (Figures S2A–2D). In addition, Y-maze testing memory consolidation showed no significant differences between Sox10^{Cre}-MCT1^{lox} animals and MCT1^{lox} controls (Figure S2E). Sox10^{Cre}-MCT1^{lox} mice spent more time in the open arms of the elevated plus maze (Figure S2H), which is indicative of reduced anxiety levels; however, no difference in anxiety in

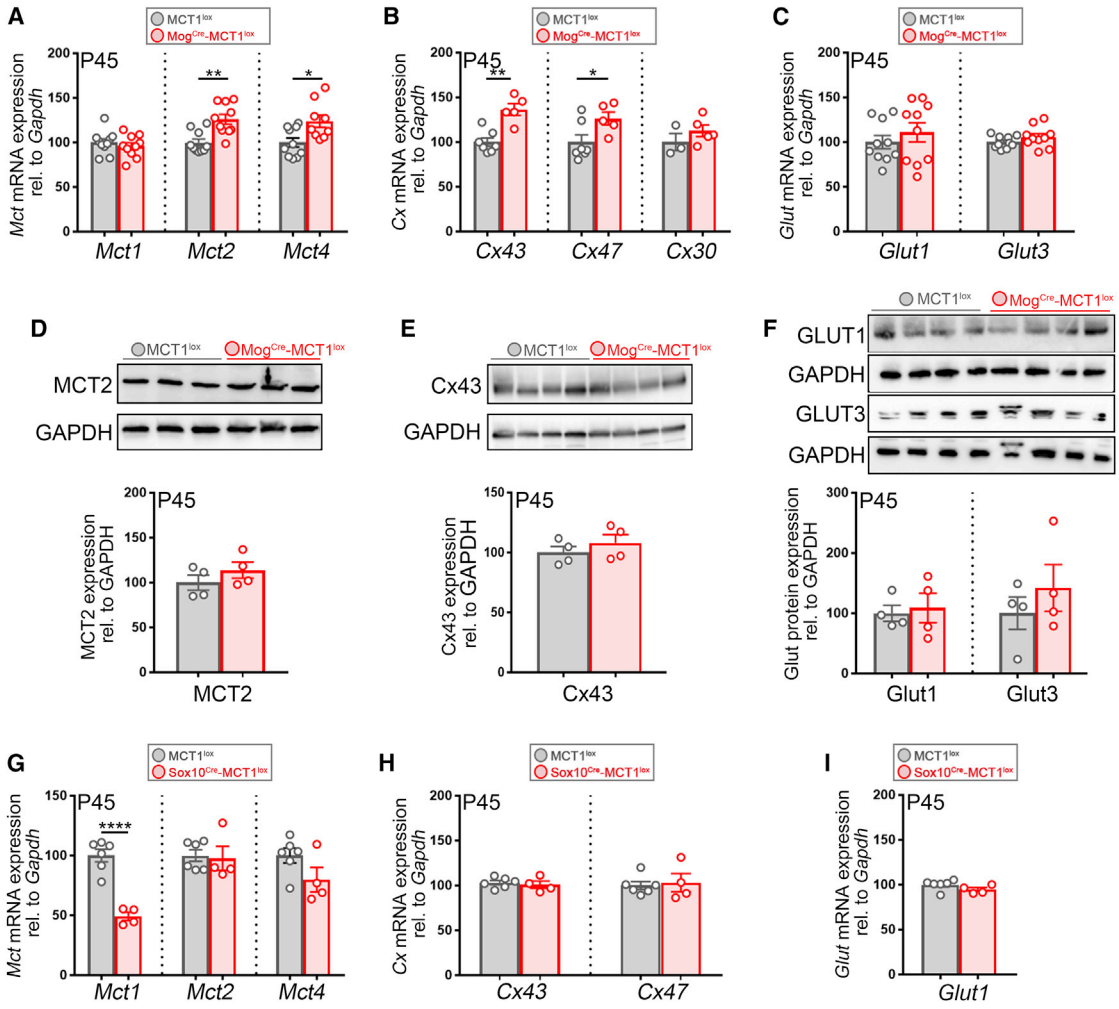

Figure 3. Conditional Loss of MCT1 in OLs Has Subtle Effects on the mRNA, but Not Protein, Expression of Other MCTs and Connexin Hemichannels

(A–C) *Mct*, connexin, and *Glut* mRNA expression in the spinal cord of P45 Mog^{Cre}-MCT1^{lox} and MCT1^{lox} mice. *Mct2* mRNA expression is elevated by 26% and *Mct4* expression by 24% in the conditional nulls, whereas *Mct1* mRNA expression is unchanged (n = 9–10, **p < 0.01, *p < 0.05, Student's t test) (A). *Cx43* hemichannel mRNA expression is increased by 27% and *Cx47* is increased by 30% in the Mog^{Cre}-MCT1^{lox} mice compared with the MCT1^{lox} controls (n = 5–7, **p < 0.01, *p < 0.05, Student's t test) (B). There are no changes in expression for glucose transporter 1 (*Glut1*) and glucose transporter 3 (*Glut3*) (n = 10) (C). Data are represented as mean ± SEM.

(D–F) Western blot on whole spinal cord protein lysates from P45 Mog^{Cre}-MCT1^{lox} and MCT1^{lox} controls does not reveal changes in the expression of MCT2 (D), Cx43 (E), and GLUT1 and GLUT3 (F) (n = 4). Data are represented as mean ± SEM.

(G–I) *Mct*, connexin, and *Glut1* mRNA expression in whole spinal cord extracts from P45 Sox10^{Cre}-MCT1^{lox} and MCT1^{lox} controls. There is a 51% reduction in *Mct1* mRNA, but no changes in *Mct2* or *Mct4*, in the conditional nulls (n = 4–6, ****p < 0.0001, Student's t test) (G). There are no changes in mRNA expression of *Cx43* and *Cx47* (H) or *Glut1* (I) (n = 4–6). Data are represented as mean ± SEM.

the open field test was observed (Figure S2D). In addition, passive avoidance test or fear trace conditioning testing did not reveal significant differences in long-term memory consolidation between Sox10^{Cre}-MCT1^{lox} and MCT1^{lox} controls (Figures S2G and S2I). In summary, behavior testing at the age of P90 in Sox10^{Cre}-MCT1^{lox} mice was mostly indistinguishable from their littermate MCT1^{lox} transgenic controls. Given that targeting MCT1 or the flow of glycogen-derived lactate from glia to neurons causes memory retention deficits and alterations in dendritic spine density (Suzuki et al., 2011; Vezzoli et al., 2019), we performed spine density measurements in Mog^{Cre}-MCT1^{lox} and MCT1^{lox} mice up to the age of P550 and found no differences in cortical or hippocampal spine density (Figure S2J). Therefore, our studies targeting MCT1 in OL lineage cells specifically do not support a role for OL MCT1 in memory retention.

We next examined multiple CNS areas of the Sox10^{Cre}-MCT1^{lox} mice for pathological changes indicative of either axonal degeneration or dysregulation of myelination. At P45, there were no signs of reactive astrogliosis or microglial activation in either cortex, spinal cord, or cerebellum (Figure 4A; data not shown).

Transmission electron microscopy (TEM) analysis was performed on isolated optic nerves sections from both genotypes to examine more subtle signs of axonal degeneration. The optic nerve was chosen for our analysis as a CNS region with high density of small myelinated axons with active OL turnover (Tripathi et al., 2017). There were no significant differences in the number of actively degenerating or degenerated axons between P45-old Sox10^{Cre}-MCT1^{lox} mice and MCT1^{lox} controls (Figure 4B). In addition, there were no differences in mitochondrial morphological parameters at either P18 or P45 (Figures S3A–S3C).

As myelination is an energetically expensive process, it could exert a significant metabolic burden on OLs during rounds of *de novo* myelination. In order to understand the influence of MCT1 loss on oligodendrogenesis and myelination, P15 Sox10^{Cre}-MCT1^{lox} and MCT1^{lox} mice were injected with 5-ethynyl-2′-deoxyuridine (EdU) for six consecutive days to label proliferating OPCs, which is a hallmark of ongoing oligodendrogenesis as well as a response to OL injury (Kang et al., 2013; Philips et al., 2013). We did not observe a significant difference in EdU^{+} OPCs in different CNS regions such as spinal cord, corpus callosum, and cortex from Sox10^{Cre}-MCT1^{lox} and MCT1^{lox} mice (Figure 4C). In addition, CC1^{+} OL cell count in the gray and white matter lumbar spinal cord areas of P45-old Sox10^{Cre}-MCT1^{lox} and MCT1^{lox} mice did not reveal significant differences (Figure 4D). Myelin thickness in optic nerve was comparable between Sox10^{Cre}-MCT1^{lox} and MCT1^{lox} mice at both P18 and P45 (Figure 4E). No changes in major myelin protein levels were detected in myelin fractions prepared from cortices of P90 Sox10^{Cre}-MCT1^{lox} mice or spinal cords of P30 Mog^{Cre}-MCT1^{lox} mice (Figures S3D and S3E). In summary, these data suggest that monocarboxylates such as lactate and pyruvate are not essential nutrients during early myelination.

OL Lineage MCT1 Null Mice Develop *Late*-Onset Axonal Degeneration and Hypomyelination

Having established that OL MCT1 is not required for energy homeostasis during early myelination and early adulthood, we evaluated pathological abnormalities in the CNS regions of conditional null mice at a more advanced age. In the OL lineage null Sox10^{Cre}-MCT1^{lox} mice at P270, there were no changes observed in the expression of microglial ionized calcium binding adaptor molecule 1 (Iba1) or astrocytic glial fibrillary acidic protein (GFAP) in the cortex, spinal cord, or cerebellum or changes in the density of cortical neurons (Figures S4A and S4C). Similar results were obtained in the Mog^{Cre}-MCT1^{lox} mice (Figures S4B and S4D). Optic nerve myelin integrity in Sox10^{Cre}-MCT1^{lox} mice appeared normal up to the age of P180 compared with MCT1^{lox} controls (Figure S5A). Lastly, quantification of aspartoacylase (ASPA)$^{+}$ OL cell number in the gray matter spinal cord showed no significant differences between P270 Mog^{Cre}-MCT1^{lox} mice and MCT1^{lox} controls (Figure S5A). These data suggest that despite the earlier reported axonal degenerative changes in the 8-month-old het *Mct1* null mice, conditional loss of *Mct1* using either Sox10^{Cre} or Mog^{Cre} does not lead to overt gliosis or axonal degeneration up to the age of P270.

Intriguingly, pathological changes were observed in multiple CNS areas in Sox10^{Cre}-MCT1^{lox} mice at P360 when mice are considered middle age, equivalent to a human age of 38–47 years (Flurkey et al., 2007). Patches of increased microglial reactivity suggestive of underlying injury were found throughout spinal cord, cerebellum, and brain stem of the Sox10^{Cre}-MCT1^{lox} mice compared with the age-matched MCT1^{lox} controls (Figures 5A–5E). Clusters of Iba1^{+}lysosomal associated membrane protein-2 (LAMP-2)$^{+}$ microglia with amoeboid "reactive" morphology were often found scattered throughout white matter areas along the rostro-caudal axis but absent from the corpus callosum (Figures 5A–5E, insets). Quantification of these clustered reactive microglia showed a 2.7-fold increase in the lumbar spinal cord in P360 Sox10^{Cre}-MCT1^{lox} mice (Figure 5F). Cerebellum white matter had a 1.6-fold increase in the number of clustered Iba1^{+}-reactive microglia (Figure 5F). Interestingly, changes in astroglial reactivity were not observed in these regions, indicative of the subtle nature of these pathological findings (Figures 5A–5E, insets). In addition, OL numbers were not affected in different CNS regions of P360 Sox10^{Cre}-MCT1^{lox} and MCT1^{lox} mice (Figure 5G).

As axonal degeneration is observed in optic nerves isolated from 8-month-old *Mct1* het mice (Lee et al., 2012), we addressed whether optic nerve axons in aged Sox10^{Cre}-MCT1^{lox} mice were degenerating as well. Optic nerves were isolated from P360 Sox10^{Cre}-MCT1^{lox} mice and MCT1^{lox} age-matched controls and processed for TEM. Image analysis revealed the presence of optic nerve axons with accumulations of swollen, intracellular organelles, indicative of active axonal degeneration. Degenerated axons were also detected with accumulation of redundant myelin loops (myelin ovoids, Figure 6A). The prevalence of these actively degenerating and degenerated axons increased 3.8-fold by P360 in Sox10^{Cre}-MCT1^{lox} mice compared with MCT1^{lox} controls (Figure 6B). In addition, some mitochondria were enlarged and had lost their typical cristae structure (Figure 6C), but this increase in mitochondrial size did not reach statistical significance (Figure 6B; Figure S5B). Furthermore, there were no changes in the number of mitochondria (Figure S5C). From P360 onward, the g-ratio (ratio between inner and outer diameter of a fiber) was increased in the Sox10^{Cre}-MCT1^{lox} optic nerves and there was a 3.2-fold increase in the proportion of hypomyelinated axons (Figure 6C). Nevertheless, the analysis of myelin isolated from the whole brain from P360-old Sox10^{Cre}-MCT1^{lox} mice revealed normal expression of abundantly expressed myelin proteins, except for a significant increase in the expression of myelin proteolipid protein (PLP) (Figure 6D).

In order to explore the physiologic consequences of MCT1 loss in the OL lineage of P360-old Sox10^{Cre}-MCT1^{lox} mice, compound action potential (CAP) recordings were performed on acutely isolated optic nerves from P360 Sox10^{Cre}-MCT1^{lox} and MCT1^{lox} mice. Optic nerves were subject to high-frequency (100-Hz) stimulation (HFS) for 30 s after an initial baseline recording period (0.1 Hz), followed by a 5-min recovery period (0.1 Hz). CAP waveforms recorded at baseline and during recovery appeared very similar between P360 MCT1^{lox} and Sox10^{Cre}-MCT1^{lox} control nerves (Figure S6A). A trend toward a delayed recovery in normalized amplitude was observed in the Sox10^{Cre}-MCT1^{lox} nerves compared with MCT1^{lox} controls, but this did not reach statistical significance (Figures S6B and S6C). In addition, despite the accumulation of hypomyelinated axons as observed with TEM, there was only a trend in reduced peak conduction velocity in the

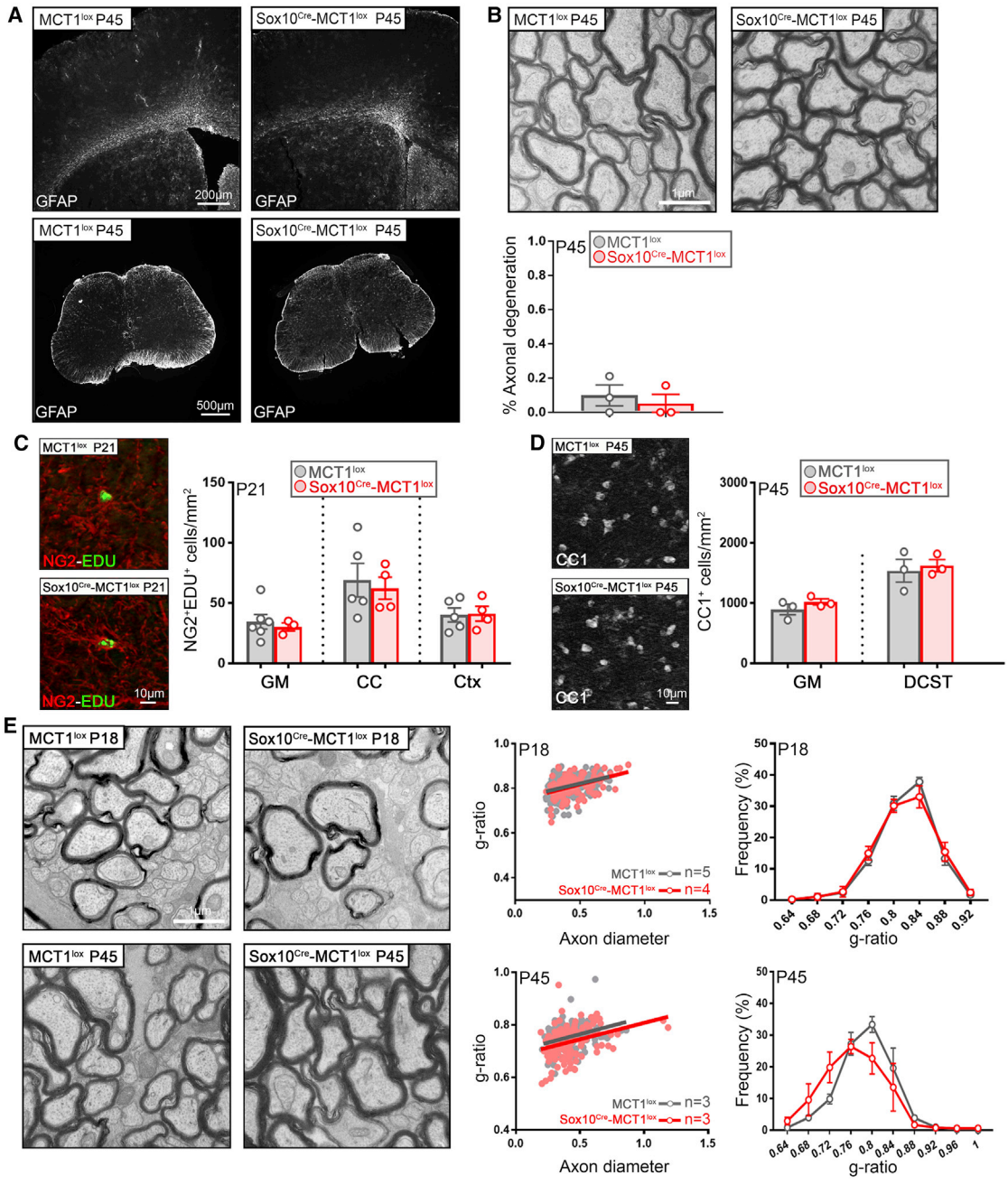

Figure 4. MCT1 Is Dispensable for Early Development and Myelination

(A) GFAP immunolabeling in Ctx, subcortical white matter (WM), and lumbar spinal cord is unaffected in P45 Sox10^{Cre}-MCT1^{lox} and MCT1^{lox} mice (representative of n = 3). Data are represented as mean ± SEM.

(B) Electron microscopic evaluation of axonal integrity in the optic nerves of P45 Sox10^{Cre}-MCT1^{lox} and MCT1^{lox} mice does not reveal significant differences (n = 3). Data are represented as mean ± SEM.

(C) Quantification of proliferating OPCs (NG2^{+}EdU^{+}) in the gray matter (GM), corpus callosum (CC), and Ctx of P21 Sox10^{Cre}-MCT1^{lox} and MCT1^{lox} mice does not reveal changes in OPC proliferation (n = 3–6). Data are represented as mean ± SEM.

(D) There are no differences in the number of CC1^{+} OLs in spinal cord GM and dorso-corticospinal tract (DCST) of P45 Sox10^{Cre}-MCT1^{lox} and MCT1^{lox} mice (n = 3). Data are represented as mean ± SEM.

(E) Myelin integrity in P18- and P45-old Sox10^{Cre}-MCT1^{lox} is maintained compared with MCT1^{lox} mice (n = 3–5). Data are represented as mean ± SEM.

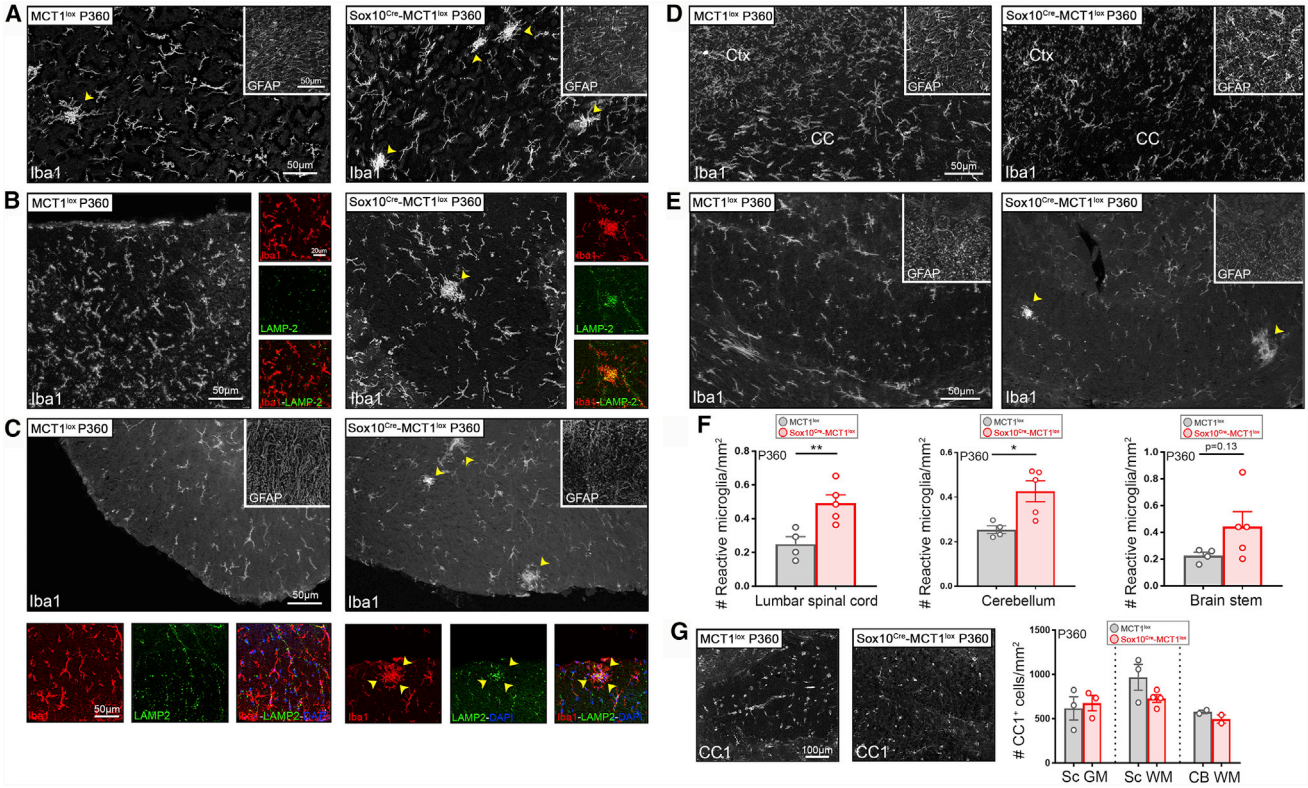

Figure 5. Increased Microglial Reactivity in the CNS WM of Aged Sox10^{Cre}-MCT1^{lox} Mice

(A–E) Microglial Iba1$^+$ reactivity is enhanced in the cerebellum (A), DCST (B), and ventral spinal cord WM (C) of P360 Sox10^{Cre}-MCT1^{lox} mice compared with MCT1^{lox} controls (arrowheads). Iba1$^+$ immunoreactivity co-localized with LAMP-2 (Mac 3), confirming that microglia acquire a more reactive phenotype (small panels taken from larger images in B and C). There was no change in GFAP immunoreactivity (insets). Microglial Iba1$^+$ and astrocyte GFAP$^+$ reactivity in the Ctx and CC of P360 Sox10^{Cre}-MCT1^{lox} is unaffected compared with MCT1^{lox} controls (D). Images are representative of n = 4–5.

(F) Quantification of changes in microglial Iba1$^+$ reactivity reveals a 2-fold increase in the spinal cord and a 1.7-fold increase in the cerebellum of P360 Sox10^{Cre}-MCT1^{lox} mice compared with MCT1^{lox} controls (spinal cord: $^{**}p < 0.01$; cerebellum: $^{*}p < 0.05$; n = 4–5, Student's t test). No change in the number of reactive microglia was observed in the brain stem (n = 4–5). Data are represented as mean ± SEM.

(G) There are no differences in the number of CC1$^+$ OL cell number in the GM spinal cord (Sc GM), WM spinal cord (Sc WM), and WM cerebellum (CB WM) between P360 Sox10^{Cre}-MCT1^{lox} and MCT1^{lox} mice (n = 2–4). Data are represented as mean ± SEM.

Sox10^{Cre}-MCT1^{lox} compared with the MCT1^{lox} controls (Figure S6D). Interestingly, all optic nerves with slowest amplitude recovery and conduction velocity values were Sox10^{Cre}-MCT1^{lox} conditional nulls, suggestive of a bimodal distribution for both parameters in the conditional null cohort, in correspondence with the findings from the EM analysis. In summary, loss of MCT1 expression in the OL lineage causes subtle axonal degeneration and hypomyelination by P360 that could impact axons already at metabolic risk during aging.

Loss of MCT1 in Mature OLs Causes Severe *Late*-Onset Axonal Degeneration

In order to understand the contribution of MCT1 in mature OLs to provide metabolic support to neurons, we performed EM on Mog^{Cre}-MCT1^{lox} mice at the ages of P90, P360, and P750. Only at the age of P750 did we detect profound axonal degeneration in optic nerves in the Mog^{Cre}-MCT1^{lox} conditional null mice compared with MCT1^{lox} controls (Figures 7A–7D). These pathological findings included "dark axons," axons containing multivesicular bodies, and redundant myelin loops scattered throughout the optic nerve, all reflective of active axonal degeneration (Figure 7A). The percentage of degenerated axons increased by 2.6-fold by P750 in the Mog^{Cre}-MCT1^{lox} mice (Figure 7D). This did not lead to differences in the axonal diameter distribution, indicating that axons were lost irrespective of caliber (Figure S7B). Overall, ~5% of all optic nerve axons were undergoing active neurodegeneration at the time of sacrifice (Figure 7D). The mitochondrial average size was increased 1.6-fold in the Mog^{Cre}-MCT1^{lox} mice, and individual mitochondria often appeared swollen, with loss of normal cristae structures, all indicative of mitochondrial metabolic disturbances (Figures 7A and 7B; Figure S7A). In addition, clusters containing swollen mitochondria increased 2.2-fold in the P750 Mog^{Cre}-MCT1^{lox} mice compared with controls (Figure 7C). Interestingly, axonal degeneration was not observed in the Mog^{Cre}-MCT1^{lox} conditional nulls at the earlier time points, either at P360 or P90, suggesting that this is a very late-onset phenomenon (Figures 7A–7D). There was no significant difference in myelin

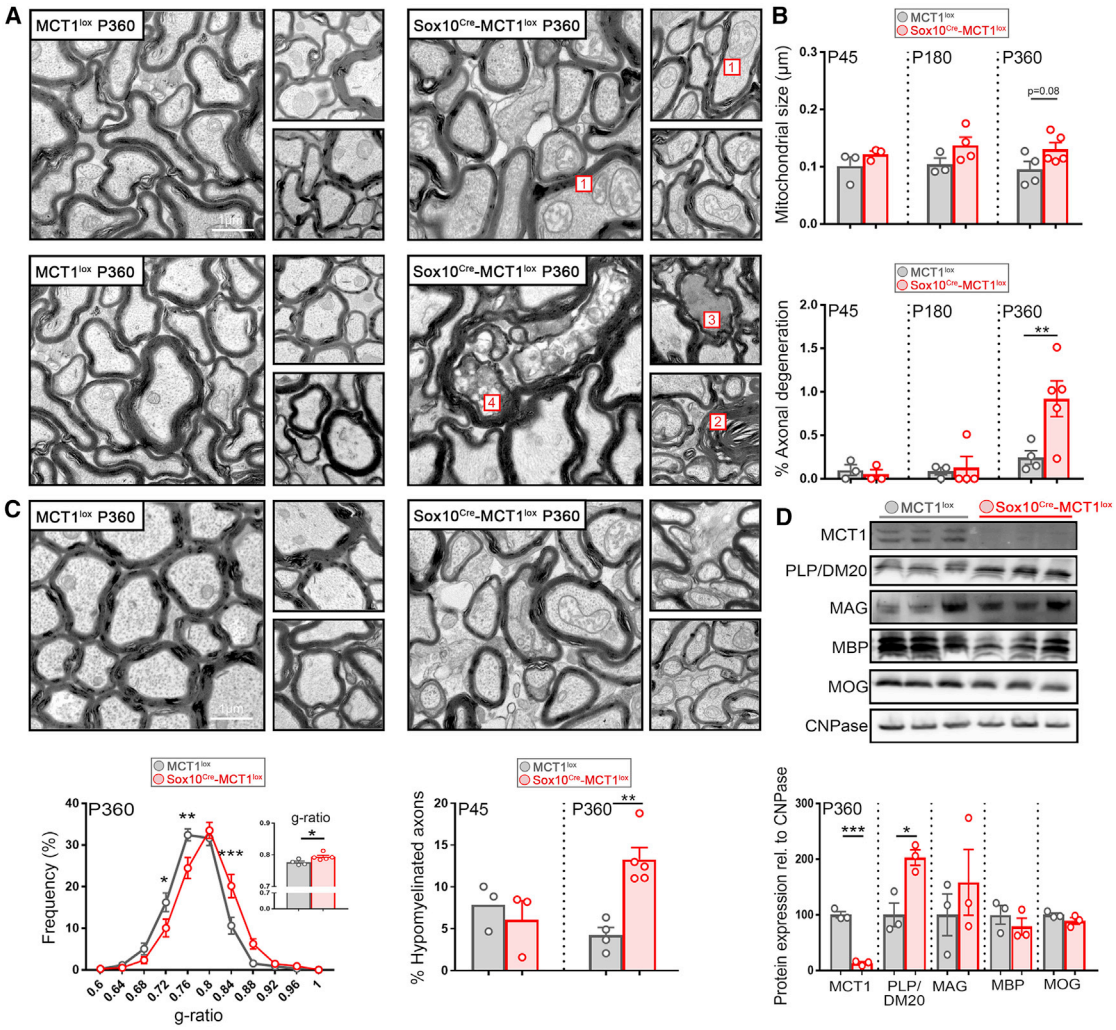

Figure 6. Axonal Degeneration and Hypomyelination in Optic Nerves Isolated from P360 Sox10^{Cre}-MCT1^{lox} Mice

(A) Electron microscopy images from P360 optic nerves from Sox10^{Cre}-MCT1^{lox} reveals the presence of enlarged mitochondria with abnormalities in christae structure (1), accumulation of redundant myelin loops (2), and active degenerating (3) as well as degenerated (4) axons containing multivesicular structures.

(B) Quantification of mitochondrial size in optic nerves of P45, P180, and P360 Sox10^{Cre}-MCT1^{lox} mice does not reveal differences compared with MCT1^{lox} littermate controls. Quantification of axonal degeneration revealed a 3.8-fold increase in the number of degenerating axons at P360 in the Sox10^{Cre}-MCT1^{lox} mice (n = 3–5, **p < 0.01, two-way ANOVA with Šidák's multiple comparison test). Data are represented as mean ± SEM.

(C) Analysis of myelin integrity in P360 Sox10^{Cre}-MCT1^{lox} and MCT1^{lox} mice reveals an increase in the abundance of thinly myelinated axons in Sox10^{Cre}-MCT1^{lox} compared with MCT1^{lox} controls (n = 4–5, *p < 0.05, **p < 0.01, ***p < 0.001, two-way ANOVA with Šidák's multiple comparison test). The g-ratio was increased in the Sox10^{Cre}-MCT1^{lox} mice (0.776 ± 0.004 in MCT1^{lox} versus 0.794 ± 0.005, n = 4–5, *p < 0.05, Student's t test). At P360, there was a 3.2-fold increase in the percentage of hypomyelinated axons (g-ratio > 0.85) in the Sox10^{Cre}-MCT1^{lox} mice compared with the MCT1^{lox} controls (n = 3–5, **p < 0.01, two-way ANOVA with Šidák's multiple comparison test). Data are represented as mean ± SEM.

(D) Western blot of myelin proteins in total brain derived myelin extracts from P360 Sox10^{Cre}-MCT1^{lox} and MCT1^{lox} mice. MCT1 expression was lowered by 87% in the Sox10^{Cre}-MCT1^{lox} mice compared with controls (n = 3, ***p < 0.001, Student's t test). PLP/DM20 expression was increased by 2-fold in the Sox10^{Cre}-MCT1^{lox} group compared with controls (n = 3, *p < 0.05, Student's t test). Expression is normalized to 2′,3′-cyclic nucleotide 3′-phosphodiesterase (CNPase). Data are represented as mean ± SEM.

thickness between Mog^{Cre}-MCT1^{lox} and MCT1^{lox} mice at P90 or P750 (Figure 7E), suggesting that the axonal degeneration observed in the Mog^{Cre}-MCT1^{lox} mice at P750 is not due to hypomyelination. In summary, these data highlight the essential role for OLs in providing neurons with metabolic support at advanced age and that loss of MCT1 at this age is an additional risk factor for developing axonal degeneration.

DISCUSSION

MCT1 Importance for Myelination

This study focused on the importance of OL lineage MCT1 in providing metabolic support to OL and neurons during aging. A key observation from this study is that MCT1 expression from OL lineage cells is not required for myelination and neuronal

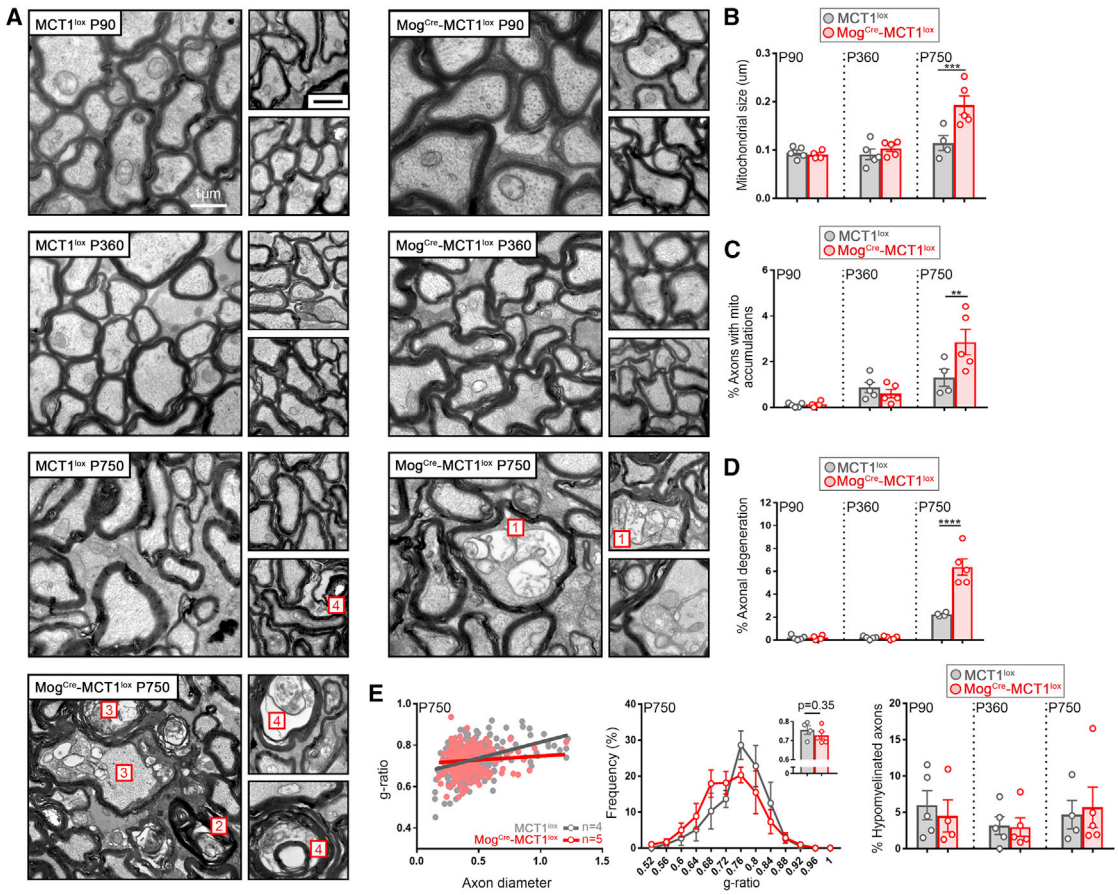

Figure 7. Age-Dependent Axonal Degeneration in Optic Nerves Isolated from Mog^{Cre}-MCT1^{lox} Mice

(A) Electron microscopy images from P750 optic nerves from Mog^{Cre}-MCT1^{lox} reveal the presence of swollen mitochondria (1), accumulation of redundant myelin loops (2), and active degenerating (3) as well as degenerated (4) axons containing multivesicular structures. These morphological changes were only rarely observed in the age-matched MCT1^{lox} controls.

(B–D) At P750, mitochondrial size is 1.7-fold increased in the Mog^{Cre}-MCT1^{lox} mice compared with the MCT1^{lox} controls (B), the accumulation of intra-axonal mitochondria is 2.2-fold increased in the Mog^{Cre}-MCT1^{lox} mice compared with the MCT1^{lox} controls (C), and the extent of axonal degeneration is 2.9-fold increased in the Mog^{Cre}-MCT1^{lox} mice compared with the MCT1^{lox} controls (D) (n = 4–5, **p < 0.01, ***p < 0.01, ****p < 0.0001, two-way ANOVA with Šidák's multiple comparison test). Data are represented as mean ± SEM.

(E) Evaluation of myelin thickness in P90- and P750-old Mog^{Cre}-MCT1^{lox} mice does not reveal changes in g-ratio, g-ratio distribution, or percentage of hypomyelinated axons (g-ratio > 0.85 [n = 4–5]). Data are represented as mean ± SEM.

energy homeostasis during development and the mature adult stage (3–6 months). However, when mice are middle age (10–14 months old), OL lineage MCT1 loss causes hypomyelination and axonal degeneration, which dramatically worsens in older age (18–24 months) (Flurkey et al., 2007). Unexpectedly, hypomyelination was not observed when MCT1 is ablated specifically in mature OLs, suggesting that expression of MCT1 in maturing OL progenitor cells is critical for myelination in aging brain. Earlier studies suggested an important role for the MCT1 substrate lactate during OL myelination, and lactate metabolism contributes to lipid biosynthesis in OLs (Ichihara et al., 2017; Rinholm et al., 2011; Sánchez-Abarca et al., 2001). Loss of MCT1 would limit lactate/pyruvate uptake and deprive OLs from the energy necessary for proper myelination. However, direct *in vivo* evidence for the role of OL MCT1 in OL myelination had not been obtained to date. Our *in vivo* observations clearly indicate that when either OLs or their progenitor cells lack MCT1, developmental myelination is unaffected during the early postnatal stages and into early adulthood, possibly due to the availability of other energy intermediates such as glucose. By contrast, the loss of MCT1 in maturing OL progenitors causes hypomyelination, potentially in concert with other age-related factors that affect the ability of OPCs to fully mature (Kang et al., 2013, Philips et al., 2013). It would be of interest to test this hypothesis in animal models of demyelination and/or limited energy intermediates to determine the consequences of MCT1 loss in the OL lineage for remyelination at either young or advanced age. With the hypomyelination observed in our OL lineage conditional nulls, there was a concomitant increase in expression of myelin proteolipid protein PLP. It remains to be explored whether the hypomyelination observed in the aged Sox10^{Cre}-MCT1^{lox} animals is due to loss of metabolites essential for myelination at this age,

changes in PLP expression, or a different, yet unknown mechanism.

Interestingly, our recent study using the same conditional MCT1 null approach indicates that P0 Cre-mediated Schwann cell MCT1 depletion leads to adult-onset hypomyelination in sensory dorsal root and sural peripheral nerves, but not in motor peripheral nerves (Jha et al., 2020). The hypomyelination occurred much earlier than in OL lineage MCT1 knockout (4 months versus 1 year of age) and leads to deficits in mechanical sensitivity by 1 year of age. Unlike OL lineage MCT1 null, hypomyelination in the Schwann cell MCT1 conditional nulls was not concomitant with axonal degeneration with aging, at least up to 1 year. A second study using an independently generated MCT1 conditional null line, also induced Schwann cell depletion of MCT1 using myelin protein zero-Cre mice (Boucanova et al., 2020), which lead to changes in motor neuron endplate innervation and altered motor neuron transcriptome. Similar to what is observed with OL lineage nulls, the phenotypes in both of these transgenic mice were relatively mild, suggesting that other metabolic transporters could compensate for the loss of MCT1 in the myelinating cells.

MCT1 and Late-Onset Axonal Degeneration

In addition to the importance of MCT1 in myelination with advanced age, our results indicate that the loss of MCT1 expression in OL lineage cells causes late-onset axonal degeneration, beyond the age of P360. During development and early postnatal life, the conditional null mice do not develop axonal degeneration, gliosis, or gross behavioral deficits and are indistinguishable from their littermate controls. We did observe significant differences when performing elevated plus maze, a test commonly used to test for anxiety, suggesting that the MCT1 conditional nulls are less anxious than their littermate controls. However, this finding was not confirmed by measuring anxiety in the open field test, where no differences were observed in time spent in the central versus peripheral area and therefore is not indicative of potential anxiety differences. Therefore, the potential impact of oligodendroglial MCT1 on anxiety remains unresolved. A previous study suggested that loss of MCT1 in hippocampal neurons of MCT1 het null mice leads to learning deficits in a specific long-term memory task (Tadi et al., 2015). In addition, rats that had MCT1 antisense oligonucleotides injected into the hippocampus developed deficits in memory retention (Suzuki et al., 2011). In our study, we did not observe learning deficits in our Sox10^{Cre}-MCT1^{lox} conditional null line when tested with passive avoidance testing, Y-maze, or fear trace conditioning testing. Regardless of differences in species and strain backgrounds used in the different studies, our data would suggest that OL lineage MCT1 is not important for memory retention compared with MCT1 expression in other cells such as astrocytes in which glycogenolysis is critical in the molecular and synaptic changes underlying memory retention (Suzuki et al., 2011; Vezzoli et al., 2019). These glycogen stores are most strongly associated with astrocytes, not OLs, and astrocyte-derived glycogen when converted to glucose and lactate could bypass the need for OL-derived lactate in providing the metabolic support needed during memory retention. Alternatively, knockdown of MCT1 in multiple cell types (OLs, astrocytes, and endothelial cells), as shown in previously published reports, may work in concert to regulate memory retention in this particular task. Studies selectively knocking out MCT1 in other cell types such as astrocytes and endothelial cells are critical to elucidate each individual contribution to memory formation through MCT1-mediated lactate release.

Of note is the delayed degeneration we observed in the Mog^{Cre}-MCT1^{lox} conditional null compared with the Sox10^{Cre}-MCT1^{lox} conditional null mice. Axonal degeneration was only observed after ~2 years of age in the Mog^{Cre}-MCT1^{lox} animals, whereas the Sox10^{Cre}-MCT1^{lox} animals developed axonal degeneration already by P360. Multiple hypotheses could explain this difference: hypomyelination, which is only observed in the Sox10^{Cre}-MCT1^{lox} line, could accelerate axonal degeneration in this line compared with the Mog^{Cre} transgenic line. Alternatively, changes in expression in connexin hemichannels or other MCTs could metabolically compensate for the loss of MCT1, but this appears less likely as only subtle changes at the mRNA level were observed in the Mog^{Cre}MCT1^{lox} mice, but not with the Sox10^{Cre}-MCT1^{lox} mice.

Axonal Degeneration in the Conditional Nulls: Comparison with Prior Findings

The onset of axonal degeneration in our conditional nulls as assessed with EM was developed at middle age (10–14 months). Although the electrophysiological CAP recording data did not reach statistical significance, the bimodal distribution of the amplitude recovery data in the conditional nulls, but not the controls, clearly indicates that degenerative changes have developed. These data could be considered confusing in light of our earlier observations in *Mct1* het null mice and mice with targeted delivery of lentiviral vectors targeting *Mct1* (Lee et al., 2012) (Table S2). In the *Mct1* het null mice, axonal degeneration was observed from the age of 8 months onward. The earlier phenotype observed in these mice could be explained by the fact that MCT1 protein is expressed in multiple cell types as clearly demonstrated by our immunostainings with a new polyclonal antibody directed at the C-terminal end of MCT1. The contribution of OL MCT1 to the phenotype observed in these *Mct1* het null mice is therefore uncertain. On the other hand, in the lentiviral injection experiments, where MCT1 is targeted with shRNA expressed under either a ubiquitous or OL-specific promoter, onset of degeneration is acute and very profound (Lee et al., 2012). Of note, the injection techniques in those prior experiments produced distinct degeneration in the control injected optic nerves and spinal cord, suggesting that a pre-injury condition might propel axonal degeneration when MCT1 expression is downregulated. Additionally, these viral injections cause local inflammation that could also alter the OL metabolic demands. This is consistent with the far milder phenotype without prior CNS damage, as occurs in the *Mct1* het null mice as well our conditional MCT1 null experiments (Lee et al., 2012). In addition, the conditional null mice experiments allow us to assess pathology at advanced age (e.g., up to P750 in the Mog^{Cre}-MCT1^{lox} mice) and throughout the entire CNS, as opposed to just locally near the site of lentivirus injection. It is only with advanced age that OL MCT1 becomes essential for providing neuronal trophic

support, potentially due to other risk factors for degeneration that become more prominent with aging, such as abnormalities in neuronal mitochondrial energy homeostasis and autophagic flux (Salvadores et al., 2017; Mattson and Magnus, 2006). Interesting, in this light, MCT1 expression is reduced in normal aging and may enhance the risk of developing neurodegeneration. Aging is, in fact, the number one risk factor in the development of neurodegenerative diseases. The death and degeneration of OLs that we and others have reported in these age-dependent diseases, as well as in their animal models, could consequently severely affect MCT1 expression levels and contribute to developing neuronal degeneration (Kang et al., 2013; Philips et al., 2013; Patel and Balabanov, 2012; Ettle et al., 2016).

In summary, we have found that OL MCT1 expression is not required for normal energy homeostasis during early development, while in adulthood, from middle-age onward, loss of OL MCT1 leads to axonopathy and hypomyelination. These data indicate that monocarboxylates such as lactate and pyruvate have an essential role in OL and neuronal energy homeostasis with advanced age and that loss of transporter expression, as observed in the normal-aging CNS and models of neurodegenerative diseases, could contribute to severe axonal injury and degeneration.

STAR★METHODS

Detailed methods are provided in the online version of this paper and include the following:

- KEY RESOURCES TABLE
- RESOURCE AVAILABILITY
  - Lead Contact
  - Materials Availability
  - Data and Code Availability
- EXPERIMENTAL MODEL AND SUBJECT DETAILS
  - Mice
  - Primary oligodendrocyte cultures
- METHOD DETAILS
  - Crossing of transgenic mouse lines
  - Animal behavior and treatment procedures
  - Assays
  - Electrophysiological recording
- QUANTIFICATION AND STATISTICAL ANALYSIS
  - Image and data analysis
  - Statistics

SUPPLEMENTAL INFORMATION

Supplemental Information can be found online at https://doi.org/10.1016/j.celrep.2020.108610.

ACKNOWLEDGMENTS

This work was funded by the Muscular Dystrophy Association (MDA, development grant 381190) (T.P.), ALS Association (J.D.R.), Department of Defense (J.D.R.), and NIH (J.D.R. and B.M.M.). We thank Carol Cooke for her help with the EM at the Neurology-Peripheral Nerve Division at Johns Hopkins University School of Medicine. We thank members of J.D.R.'s lab at Johns Hopkins University School of Medicine for helpful discussions.

AUTHOR CONTRIBUTIONS

T.P. designed, performed, and analyzed experiments and wrote the manuscript. Y.A.M. performed the electrophysiology experiments and data analysis, which was overseen by D.E.B. Y.J. and M.V.P. assisted with design and data interpretation of the mouse behavioral experiments. S.V. performed the lactate and pyruvate uptake assays. M.H.F. assisted with EM imaging and data analysis. B.M.M. and J.D.R. oversaw the project development, execution, and manuscript writing.

DECLARATION OF INTERESTS

The authors declare no competing interests.

Received: April 11, 2020
Revised: September 8, 2020
Accepted: December 16, 2020
Published: January 12, 2021

REFERENCES

Alberini, C.M., Cruz, E., Descalzi, G., Bessières, B., and Gao, V. (2018). Astrocyte glycogen and lactate: New insights into learning and memory mechanisms. Glia *66*, 1244–1262.

Andres Benito, P., Dominguez Gonzalez, M., and Ferrer, I. (2018). Altered gene transcription linked to astrocytes and oligodendrocytes in frontal cortex in Creutzfeldt-Jakob disease. Prion *12*, 216–225.

Argente-Arizón, P., Guerra-Cantera, S., Garcia-Segura, L.M., Argente, J., and Chowen, J.A. (2017). Glial cells and energy balance. J. Mol. Endocrinol. *58*, R59–R71.

Boucanova, F., Pollmeier, G., Sandor, K., Morado Urbina, C., Nijssen, J., Medard, J.J., Bartesaghi, L., Pellerin, L., Svensson, C.I., Hedlund, E., et al. (2020). Disrupted function of lactate transporter MCT1, but not MCT4, in Schwann cells affects the maintenance of motor end-plate innervation. Glia *69*, 124–136.

Brady, S.T., Witt, A.S., Kirkpatrick, L.L., de Waegh, S.M., Readhead, C., Tu, P.H., and Lee, V.M. (1999). Formation of compact myelin is required for maturation of the axonal cytoskeleton. J. Neurosci. *19*, 7278–7288.

Buch, T., Heppner, F.L., Tertilt, C., Heinen, T.J., Kremer, M., Wunderlich, F.T., Jung, S., and Waisman, A. (2005). A Cre-inducible diphtheria toxin receptor mediates cell lineage ablation after toxin administration. Nat. Methods *2*, 419–426.

Ettle, B., Schlachetzki, J.C.M., and Winkler, J. (2016). Oligodendroglia and Myelin in Neurodegenerative Diseases: More Than Just Bystanders? Mol. Neurobiol. *53*, 3046–3062.

Flurkey, K.C., Currer, J.M., and Harrison, D.E. (2007). Mouse models in aging research. In The Mouse in Biomedical Research, 2nd, J.G. Fox, S.W. Barthold, M.T. Davisson, C.E. Newcomer, F.W. Quimby, and A.L. Smith, eds. (Elsevier), pp. 637–672.

Fünfschilling, U., Supplie, L.M., Mahad, D., Boretius, S., Saab, A.S., Edgar, J., Brinkmann, B.G., Kassmann, C.M., Tzvetanova, I.D., Möbius, W., et al. (2012). Glycolytic oligodendrocytes maintain myelin and long-term axonal integrity. Nature *485*, 517–521.

Griffiths, I., Klugmann, M., Anderson, T., Yool, D., Thomson, C., Schwab, M.H., Schneider, A., Zimmermann, F., McCulloch, M., Nadon, N., and Nave, K.A. (1998). Axonal swellings and degeneration in mice lacking the major proteolipid of myelin. Science *280*, 1610–1613.

Ichihara, Y., Doi, T., Ryu, Y., Nagao, M., Sawada, Y., and Ogata, T. (2017). Oligodendrocyte Progenitor Cells Directly Utilize Lactate for Promoting Cell Cycling and Differentiation. J. Cell. Physiol. *232*, 986–995.

Jha, M.K., Lee, Y., Russell, K.A., Yang, F., Dastgheyb, R.M., Deme, P., Ament, X.H., Chen, W., Liu, Y., Guan, Y., et al. (2020). Monocarboxylate transporter 1 in Schwann cells contributes to maintenance of sensory nerve myelination during aging. Glia *68*, 161–177.

Jouroukhin, Y., Kageyama, Y., Misheneva, V., Shevelkin, A., Andrabi, S., Prandovszky, E., Yolken, R.H., Dawson, V.L., Dawson, T.M., Aja, S., et al. (2018). DISC1 regulates lactate metabolism in astrocytes: implications for psychiatric disorders. Transl. Psychiatry *8*, 76.

Kang, S.H., Li, Y., Fukaya, M., Lorenzini, I., Cleveland, D.W., Ostrow, L.W., Rothstein, J.D., and Bergles, D.E. (2013). Degeneration and impaired regeneration of gray matter oligodendrocytes in amyotrophic lateral sclerosis. Nat. Neurosci. *16*, 571–579.

Lappe-Siefke, C., Goebbels, S., Gravel, M., Nicksch, E., Lee, J., Braun, P.E., Griffiths, I.R., and Nave, K.A. (2003). Disruption of Cnp1 uncouples oligodendroglial functions in axonal support and myelination. Nat. Genet. *33*, 366–374.

Larson, V.A., Mironova, Y., Vanderpool, K.G., Waisman, A., Rash, J.E., Agarwal, A., and Bergles, D.E. (2018). Oligodendrocytes control potassium accumulation in white matter and seizure susceptibility. eLife *7*, e34829.

Lee, Y., Morrison, B.M., Li, Y., Lengacher, S., Farah, M.H., Hoffman, P.N., Liu, Y., Tsingalia, A., Jin, L., Zhang, P.W., et al. (2012). Oligodendroglia metabolically support axons and contribute to neurodegeneration. Nature *487*, 443–448.

Magistretti, P.J., and Allaman, I. (2018). Lactate in the brain: from metabolic end-product to signalling molecule. Nat. Rev. Neurosci. *19*, 235–249.

Mattson, M.P., and Magnus, T. (2006). Ageing and neuronal vulnerability. Nat. Rev. Neurosci. *7*, 278–294.

Patel, J., and Balabanov, R. (2012). Molecular mechanisms of oligodendrocyte injury in multiple sclerosis and experimental autoimmune encephalomyelitis. Int. J. Mol. Sci. *13*, 10647–10659.

Philips, T., Bento-Abreu, A., Nonneman, A., Haeck, W., Staats, K., Geelen, V., Hersmus, N., Küsters, B., Van Den Bosch, L., Van Damme, P., et al. (2013). Oligodendrocyte dysfunction in the pathogenesis of amyotrophic lateral sclerosis. Brain *136*, 471–482.

Pierre, K., Pellerin, L., Debernardi, R., Riederer, B.M., and Magistretti, P.J. (2000). Cell-specific localization of monocarboxylate transporters, MCT1 and MCT2, in the adult mouse brain revealed by double immunohistochemical labeling and confocal microscopy. Neuroscience *100*, 617–627.

Pletnikov, M.V., Ayhan, Y., Nikolskaia, O., Xu, Y., Ovanesov, M.V., Huang, H., Mori, S., Moran, T.H., and Ross, C.A. (2008). Inducible expression of mutant human Dros. Inf. Serv.C1 in mice is associated with brain and behavioral abnormalities reminiscent of schizophrenia. Mol. Psychiatry *13*, 173–186.

Rinholm, J.E., Hamilton, N.B., Kessaris, N., Richardson, W.D., Bergersen, L.H., and Attwell, D. (2011). Regulation of oligodendrocyte development and myelination by glucose and lactate. J. Neurosci. *31*, 538–548.

Rothstein, J.D., Martin, L., Levey, A.I., Dykes-Hoberg, M., Jin, L., Wu, D., Nash, N., and Kuncl, R.W. (1994). Localization of neuronal and glial glutamate transporters. Neuron *13*, 713–725.

Saab, A.S., and Nave, K.A. (2017). Myelin dynamics: protecting and shaping neuronal functions. Curr. Opin. Neurobiol. *47*, 104–112.

Saab, A.S., Tzvetavona, I.D., Trevisiol, A., Baltan, S., Dibaj, P., Kusch, K., Möbius, W., Goetze, B., Jahn, H.M., Huang, W., et al. (2016). Oligodendroglial NMDA Receptors Regulate Glucose Import and Axonal Energy Metabolism. Neuron *91*, 119–132.

Salvadores, N., Sanhueza, M., Manque, P., and Court, F.A. (2017). Axonal Degeneration during Aging and Its Functional Role in Neurodegenerative Disorders. Front. Neurosci. *11*, 451.

Sánchez-Abarca, L.I., Tabernero, A., and Medina, J.M. (2001). Oligodendrocytes use lactate as a source of energy and as a precursor of lipids. Glia *36*, 321–329.

Schneider, C.A., Rasband, W.S., and Eliceiri, K.W. (2012). NIH Image to ImageJ: 25 years of image analysis. Nat. Methods *9*, 671–675.

Shevelkin, A.V., Terrillion, C.E., Abazyan, B.N., Kajstura, T.J., Jouroukhin, Y.A., Rudow, G.L., Troncoso, J.C., Linden, D.J., and Pletnikov, M.V. (2017). Expression of mutant DISC1 in Purkinje cells increases their spontaneous activity and impairs cognitive and social behaviors in mice. Neurobiol. Dis. *103*, 144–153.

Stavoe, A.K.H., and Holzbaur, E.L.F. (2019). Neuronal autophagy declines substantially with age and is rescued by overexpression of WIPI2. Autophagy *16*, 371–372.

Suzuki, A., Stern, S.A., Bozdagi, O., Huntley, G.W., Walker, R.H., Magistretti, P.J., and Alberini, C.M. (2011). Astrocyte-neuron lactate transport is required for long-term memory formation. Cell *144*, 810–823.

Tadi, M., Allaman, I., Lengacher, S., Grenningloh, G., and Magistretti, P.J. (2015). Learning-Induced Gene Expression in the Hippocampus Reveals a Role of Neuron -Astrocyte Metabolic Coupling in Long Term Memory. PLoS ONE *10*, e0141568.

Tang, X., Li, Z., Zhang, W., and Yao, Z. (2019). Nitric oxide might be an inducing factor in cognitive impairment in Alzheimer's disease via downregulating the monocarboxylate transporter 1. Nitric Oxide *91*, 35–41.

Terrillion, C.E., Abazyan, B., Yang, Z., Crawford, J., Shevelkin, A.V., Jouroukhin, Y., Yoo, K.H., Cho, C.H., Roychaudhuri, R., Snyder, S.H., et al. (2017). DISC1 in Astrocytes Influences Adult Neurogenesis and Hippocampus-Dependent Behaviors in Mice. Neuropsychopharmacology *42*, 2242–2251.

Tripathi, R.B., Jackiewicz, M., McKenzie, I.A., Kougioumtzidou, E., Grist, M., and Richardson, W.D. (2017). Remarkable Stability of Myelinating Oligodendrocytes in Mice. Cell Rep. *21*, 316–323.

Vezzoli, E., Cali, C., De Roo, M., Ponzoni, L., Sogne, E., Gagnon, N., Francolini, M., Braida, D., Sala, M., Muller, D., et al. (2019). Ultrastructural Evidence for a Role of Astrocytes and Glycogen-Derived Lactate in Learning-Dependent Synaptic Stabilization. Cereb. Cortex *30*, 2114–2127.

Yin, X., Crawford, T.O., Griffin, J.W., Tu, P.h., Lee, V.M., Li, C., Roder, J., and Trapp, B.D. (1998). Myelin-associated glycoprotein is a myelin signal that modulates the caliber of myelinated axons. J. Neurosci. *18*, 1953–1962.

STAR★METHODS

KEY RESOURCES TABLE

REAGENT or RESOURCE	SOURCE	IDENTIFIER
Antibodies		
mouse monoclonal anti-APC antibody [CC-1]	Abcam	Cat#ab16794; RRID:AB_443473
mouse monoclonal anti-CNPase antibody clone 11-5B	MilliporeSigma	Cat#MAB326; RRID:AB_2082608
rabbit polyclonal anti-Connexin-43 antibody	MilliporeSigma	Cat#C6219; RRID:AB_476857
mouse monoclonal anti-GAPDH (6C5)	Thermo Fisher Scientific	Cat#AM4300; RRID:AB_437392
chicken polyclonal anti-GFAP	MilliporeSigma	Cat#AB5541; RRID:AB_10579068
rabbit polyclonal anti-GFP	Rockland Immunochemicals	Cat#600-401-215; RRID:AB_828167
rabbit polyclonal anti-Glut1	Abcam	Cat#Ab652; RRID:AB_305540
rabbit monoclonal anti-Glut3	Abcam	Cat#Ab191071; RRID:AB_2736916
rabbit polyclonal anti-Iba1	WAKO	Cat#019-19741; RRID:AB_839504
rat monoclonal anti-CD107b (LAMP-2)	Biolegend	Cat#816101; RRID:AB_2564796
mouse monoclonal anti-MAG	MilliporeSigma	Cat#MAB1567; RRID:AB_2137847
mouse monoclonal anti-MBP	Biolegend	Cat#808403; RRID:AB_2628849
chicken polyclonal anti-MCT1	Dr. Jeffrey Rothstein (Jha et al., 2020)	N/A
rabbit polyclonal anti-MCT2	MilliporeSigma	Cat#AB3542; RRID:AB_177409
mouse monoclonal anti-MOG	MilliporeSigma	Cat#MAB5680; RRID:AB_1587278
rabbit polyclonal anti-NG2	MilliporeSigma	Cat#AB5320; RRID:AB_11213678
mouse monoclonal anti-Myelin proteolipid protein clone PLPC1	MilliporeSigma	Cat#MAB388; RRID:AB_177623
rabbit anti-GLT-1	Dr. Jeffrey Rothstein (Rothstein et al., 1994)	N/A
mouse anti-CD31	BD	Cat#550389; RRID:AB_2252087
Chemicals, Peptides, and Recombinant Proteins		
AR-C155858	Tocris	Cat#4960
Lactate acid, sodium salt. L-^{14}C	PerkinElmer	Cat#NEC599050UC
Pyruvic acid, sodium salt, 1-^{14}C	PerkinElmer	Cat#NEC255050UC
Tamoxifen	MilliporeSigma	Cat#T5648
Critical Commercial Assays		
Taqman assay: Slc16a1 (MCT1)	Thermo Scientific	Cat#4331182; Mm01306378_m1
Taqman assay: Slc16a7 (MCT2)	Thermo Scientific	Cat#4331182; Mm00445115_m1
Taqman assay: mouse Slc16a3 (MCT4)	Thermo Scientific	Cat#4331182; Mm00446102_m1
Taqman assay: mouse Slc2a1 (GLUT1)	Thermo Scientific	Cat#4331182; Mm00441480_m1
Taqman assay: mouse Slc2a3 (GLUT3)	Thermo Scientific	Cat#4331182; Mm00441483_m1
Taqman assay: mouse Gjb6 (Cx30)	Thermo Scientific	Cat#4331182; Mm00433661_s1
Taqman assay: mouse Gjc2 (Cx47)	Thermo Scientific	Cat#4331182; Mm00519131_s1
Taqman assay: mouse Gja1 (Cx43)	Thermo Scientific	Cat#4331182; Mm00439105_m1
Taqman assay: mouse GAPD	Thermo Scientific	Cat#4352339E
O4 microbeads	Miltenyi	Cat#130-094-543
Adult brain dissociation kit	Miltenyi	Cat#130-107-677
Click-iT EdU Cell Proliferation Kit for Imaging, Alexa Fluor 488 dye	Thermo Scientific	Cat#C10337

(*Continued on next page*)

Continued

REAGENT or RESOURCE	SOURCE	IDENTIFIER
Experimental Models: Cell Lines		
Mouse primary oligodendrocytes ($Sox10^{Cre}$-$MCT1^{lox}$)	This paper	N/A
Mouse primary oligodendrocytes ($MCT1^{lox}$)	This paper	N/A
Experimental Models: Organisms/Strains		
Mouse: B6SJLF1/J	Jackson Laboratory	Cat#100012
Mouse: MCT1tdTomato	Dr. Jeffrey Rothstein (Lee et al., 2012)	N/A
Mouse: B6N.Cg-Tg(Pdgfra-cre/ERT) 467Dbe/J	Dr. Dwight Bergles /Jackson Laboratory	Cat#018280
Mouse: B6.129X1*Gt(ROSA)26Sor*$^{tm1(EYFP)Cos}$/J	Jackson Laboratory	Cat#006148
Mouse: $Mog^{tm1(Cre)Gkl}$	Dr. Ari Waisman (Buch et al., 2005)	http://www.informatics.jax.org/allele/MGI:3689957
Mouse: B6;CBA-Tg(Sox10-cre)1Wdr/J	Jackson laboratory	Cat#025807
Mouse: $MCT1^{lox}$	Dr. Jeffrey Rothstein (Jha et al., 2020)	N/A
Software and Algorithms		
ImageJ	Schneider et al., 2012	https://imagej.nih.gov/ij/
GraphPad Prism 7	GraphPad	https://www.graphpad.com/scientific-software/prism/
Zen 2.3 Lite	Zeiss	https://www.zeiss.com/microscopy/us/products/microscope-software/zen-lite.html
MATLAB (R2014b)	Mathworks	https://www.mathworks.com/
Clampfit 11	Molecular Devices	https://mdc.custhelp.com/app/answers/detail/a_id/20260/~/axon™-pclamp™-11-electrophysiology-data-acquisition-%26-analysis-software
Origin 2020	OriginLab	https://www.originlab.com/2020

RESOURCE AVAILABILITY

Lead Contact

Further information and requests for resources and reagents should be directed to and will be fulfilled by the Lead Contact, Jeffrey D. Rothstein (jrothstein@jhmi.edu).

Materials Availability

The MCT1 conditional null mice generated in this study will be made available upon request. We will require a Material Transfer Agreement to be completed prior to sharing.

Data and Code Availability

This study did not generate any unique datasets or code.

EXPERIMENTAL MODEL AND SUBJECT DETAILS

Mice

Non-transgenic B6SJLF1/J mice were purchased from the Jackson Laboratory (Stock No: 100012). *Mct1-tdTomato* mice were generated in our laboratory and described in our earlier study (Lee et al., 2012). *B6N.Cg-Tg(Pdgfra-cre/ERT)467Dbe/J* ((*Pdgfrα-CreER*) mice were obtained from Dr. Dwight Bergles at Johns Hopkins University. B6.129X1*Gt(ROSA)26Sor*$^{tm1(EYFP)Cos}$/J (*RosaYFP)* reporter mice were obtained from Jackson Laboratories (Stock No: 006148). *Mct1* conditional null mice ($MCT1^{lox}$) were recently generated in our laboratory (Jha et al., 2020). $Mog^{tm1(Cre)Gkl}$ (Mog^{Cre}) mice were generated by Dr. Ari Waisman from University of Mainz, Germany and kindly shared with our laboratory (Buch et al., 2005). *B6;CBA-Tg(Sox10-cre)1Wdr/J* mice ($Sox10^{Cre}$ mice) were obtained from Jackson Laboratories (Stock No: 025807). Both male and female littermates were used in this study and

randomly allocated to each of the experimental groups at ages varying from P21 to P750. All mice are kept in 14 hours light/10 hours dark cycle. All animal experiments were carried out in compliance with animal protocols approved by the Animal Care and Use Committee at the Johns Hopkins University School of Medicine.

Primary oligodendrocyte cultures

OL lineage cell cultures were prepared from P7 mouse cortices from Sox10^{Cre}-MCT1^{lox} and MCT1^{lox} mice. Both male and female pups were allocated to each experimental group. Cortices were dissociated using the adult mouse brain dissociation kit according to the manufacturer's protocol (Miltenyi). In short, meninges were removed and cortices underwent papain digestion for 30 min. using the adult brain dissociator (Miltenyi). After passage of cells through a 70μm cell strainer, myelin was removed with 'myelin debris removal solution' and single cells were pelleted. Red blood cells were removed using 'Red Blood cell Removal Solution' and cells were incubated with anti-O4 magnetic microbeads for 15 minutes on ice. O4^{+} oligodendrocyte progenitors were then magnetically sorted and collected in oligodendrocyte cell medium. O4^{+} cells derived from the same genotype and from either male or/ female pup were pooled in order to increase cell plating density. Cells were plated at 400K per well in a 6-well plate and maintained in the cell incubator at 37.5°C with 0.5% CO_2. The oligodendrocyte medium used contains DMEM-F12 with HEPES and Glutamax, N2 supplement, B27 supplement, 20ng/μl basic fibroblast growth factor (bFGF) and 20ng/μl platelet derived growth factor α (PDGFα). Cells were plated on 6-well plates that were coated overnight with Matrigel at 37.5°C and 0.5% CO_2.

METHOD DETAILS

Crossing of transgenic mouse lines

The *Pdgfrα-CreER* mice were crossed with *RosaYFP* and *Mct1-tdTomato* mice to generate triple transgenic animals, hemizygous for either transgene.

The MCT1^{lox} conditional null mice were crossed with hemizygous Mog^{Cre} or hemizygous Sox10^{Cre} mice to obtain double transgenic Mog^{Cre}-MCT1^{lox} and Sox10^{Cre}-MCT1^{lox} mice, hemizygous for Cre and homozygous for the MCT1 conditional allele. All mice used in this study were hemizygous for Cre and homozygous for the MCT1^{lox} allele.

Animal behavior and treatment procedures

All mouse behavior experiments were performed at the Johns Hopkins animal behavior core.

Accelerated Rotarod

Motor learning and coordination were examined by the rotarod test (Rotamex-5 System with a spindle dimensions of 3.0 cm x 9.5 cm; Columbus Instruments). Testing was conducted over a 3 day period, where each mouse was given three trials per day and latency to fall off the rotarod was measured as it accelerated from 4 to 99 rpm over a 5 min. period. Before the start of testing on the first day, each mouse was given a habituation trial by being placed on the rotarod, which was rotating at a constant speed of 4 rpm for 10 min. The mean latencies were calculated for each animal.

Open field testing

Spontaneous locomotion was assessed over a 30 min. period using activity chambers (16" (W) x 16" (D) x 15" (H)) with Photobeam Activity System (PAS) open field system equipped with 16 × 16 infrared beams (San Diego Instruments, San Diego, CA, USA) during the dark period from 10:00am to 06:00pm (reversed light cycle). Total locomotor activity was automatically measured as the number of beams breaks. The center zone was defined as the surface area covered by central 14 × 14 beams of the box (14 × 14 inches) with the remaining peripheral area being designated as the peripheral zone. The amount of time mice spend along the walls was used as a measure of anxiety.

Y-maze

Spatial working memory assessed by spontaneous alternation and spatial recognition memory were assessed in the y-maze test as previously described (Shevelkin et al., 2017).

Passive avoidance test

Passive avoidance was assessed using GEMINI Active and Passive Avoidance System (Stoelting Co., Wood Dale, IL). Briefly, a mouse was placed in the light compartment of the shuttle box for 30 s. to acclimate. Following the habituation, the door between two compartments was opened, and the latency to enter the dark compartment was measured. Entering the dark compartment led to closing the door. Three seconds after entering the dark compartment, the mouse was exposed to an inescapable foot shock delivered for at the intensity of 0.5mA. Twenty-four hours following the training session, the mouse was returned to the light compartment, the door between the compartments was opened and the latency to enter the dark compartment was measured. The cut-off time was 5 min.

Elevated Maze Plus

Anxiety was evaluated in the plus-maze (San Diego Instruments Inc., San Diego, CA, USA) as previously described (Pletnikov et al., 2008).

Trace fear trace conditioning test

Trace fear conditioning (TFC) was assessed as previously described (Jouroukhin et al., 2018; Terrillion et al., 2017). Briefly, TFC is a 3 day test consisting of the habituation day, training day, and test day. On day 1, a mouse was habituated to the shock box

(Coulbourn, Holliston, MA) for 10 min. On Day 2, the mouse was placed in the shock box, and a 20 s. 90dB tone was delivered. Twenty seconds following the termination of the tone, a scrambled 2 s. 0.5 mA shock was delivered. This tone-shock pairing was repeated three times. On Day 3, the mice were placed in the shock box for 3 min and the freezing behavior was assessed as a measure of contextual memory. Following the context test, the cued test was performed. The mice were placed in a different testing box, and the tone presented during the training session was presented three times. The freezing behavior in response to the tones was assessed as a measure of cue-dependent fear memory. Freezing was automatically detecting using the Freeze Scan software (Clever Sys Inc.).

Tamoxifen injections

Tamoxifen (MilliporeSigma) was dissolved in ethanol, vortexed for 10 s. and dissolved in sunflower seed oil (ratio ethanol-oil 1:10). *PDGFRαCreER* mice crossed with *RosaYFP* and *Mct1-tdTomato* mice were injected intraperitoneally with 4 doses of tamoxifen (200mg/kg) for 4 consecutive days. Four different cohorts were injected: P60-P150-P300 and P550. Mice were sacrificed 30 days after the first injection.

EDU proliferation assay

P14 old mice were injected with 5mg/kg EDU for 5 consecutive days. Mice were sacrificed one week after the first injection at P21. EDU immunostaining in different CNS areas was performed according to the manufacturer's protocol (Thermo Scientific).

Assays

Immunohistochemistry

Mice were deeply anesthetized by I.P. injections of anesthetic cocktail acepromazine maleate (3mg/kg; MWI Veterinary Supply), ketamine (100mg/kg; MWI Veterinary Supply), and xylazine (20mg/kg; MWI Veterinary Supply). Mice were transcardially perfused with ice-cold PBS followed by ice-cold PBS containing 4% paraformaldehyde (PFA). Spinal cord, cerebellum, optic nerve and forebrains were dissected and post-fixed in 4% PFA in PBS for 4 hours. Samples were stored overnight in 30% sucrose solution in PBS at 4°C and subsequently embedded in OCT compound (Sakura Finetek). 20 μm spinal cord and 40 μm coronal brain and cerebellar floating sections were cut on a cryostat (Thermo Scientific), washed in PBS and blocked for 1 hour at room temperature in PBS solution containing 0.1% Triton X-100 (PBST) and 10% normal goat serum (Vector). Sections were then incubated overnight at 4°C with primary antibodies diluted in PBST: chicken ant-MCT1 (our lab), rabbit anti- Iba1 (WAKO), rabbit anti-NG2 (MilliporeSigma), chicken anti-GFAP (MilliporeSigma), rabbit anti-GFP (Rockland), mouse anti-CC1 (Abcam), rat anti-LAMP-2 (Biolegend), mouse anti-CD31 (BD), rabbit anti-GLT-1 (our lab) and mouse anti-NeuN (MilliporeSigma)(for more details see Key Resources Table). Sections were washed in PBST and incubated with fluorescent labeled secondary antibodies (Thermo Scientific) for 1 hour at room temperature. Sections were subsequently washed in PBST and mounted on glass slides in Prolong Gold antifade reagent containing DAPI (Thermo Scientific). Section were imaged on a Zeiss Axioimager Z1 equipped with Apotome 2 or on a Zeiss 800 confocal microscope (Zeiss).

Myelin preparation

Whole brain and spinal cord were dissected and homogenized in 0.32M sucrose using an ultra-turrax homogenizer. The homogenate was carefully layered over a 0.85M sucrose solution and centrifuged at 75000 g for 30 min. at 4°C in Beckman ultracentrifuge (Beckman). After centrifugation, the myelin containing interface was collected, washed with deionized water and centrifuged at 75000 g for 15 min at 4°C. The pelleted fractions then underwent two rounds of osmotic shock by incubation in deionized water for 10 min. on ice followed by ultracentrifugation at 12000 g for 15 min. at 4°C. Pellets were then dissolved in 0.32M sucrose, layered over 0.85M sucrose and myelin containing interface was collected after centrifugation at 75000 g for 30 min. at 4°C. After another wash in deionized water, myelin was pelleted by centrifugation at 75000 g for 15 min at 4°C. Myelin pellets were dissolved in RIPA buffer (Thermo Scientific), complemented with protease and phosphatase inhibitors and stored at −80°C.

Western Blot

The protein concentration of each sample was measured using the Lowry method and the colorimetric reaction was measured on a SpectraMax M3 plate reader (Molecular Devices). 10-40μg of total protein was loaded on mini Protean TGX Precast gels (Biorad). After electrophoresis, proteins were blotted on a PVDF membrane (Biorad) and blocked in 5% Blotting Grade Blotter (Biorad) diluted in Tris buffered saline (TBS) containing 0.1% Tween 20 (TBST). Blots were then incubated with either of the following antibodies: chicken anti-human MCT1 antibody, mouse anti-PLP (MilliporeSigma), mouse anti CNPase (MilliporeSigma), rabbit anti-MCT2 (MilliporeSigma), rabbit anti-GLUT1 (abcam), rabbit anti-GLUT3 (abcam), mouse anti-MBP (Biolegend), mouse anti-MOG (MilliporeSigma), rabbit anti-Connexin-43 (MilliporeSigma), mouse anti-GAPDH (Thermo Scientific), and mouse anti-MAG (MilliporeSigma)(for more details see Key Resources Table). Membranes were overnight incubated with primary antibodies at 4°C. Membranes were washed with TBST and incubated with HRP labeled secondary antibodies for 1 hour at room temperature. After two washes in TBST and one wash in TBS, membranes were exposed to ECL reagent for 2 min. (Thermo Scientific) and chemiluminescent signal was detected with the LAS Imager 4000 (GE Healthcare).

Isolation of adult oligodendrocyte progenitor cells

P150 Sox10Cre-MCT1^{lox} and MCT1^{lox} mice were deeply anesthetized by I.P. injections of anesthetic cocktail acepromazine maleate (3mg/kg; MWI Veterinary Supply), ketamine (100mg/kg; MWI Veterinary Supply), and xylazine (20mg/kg; MWI Veterinary Supply). Mice were transcardially perfused with ice-cold PBS. Brain cortices were dissected and placed in PBS with calcium/magnesium. O4^{+} oligodendrocyte progenitors were isolated according to the adult brain dissociation protocol (Miltenyi) as outlined under 'primary

oligodendrocyte cultures' (see above). After magnetic sorting, cells were centrifuged for 5 min. at 300 g at 4°C. Pellets were dissolved in Tri Reagent (Zymo Research) and RNA was extracted using the Direct-zol RNA MicroPrep kit (Zymo Research).

Reverse transcriptase-q-PCR

Mice were deeply anesthetized by I.P. injections of anesthetic cocktail acepromazine maleate (3mg/kg; MWI Veterinary Supply), ketamine (100mg/kg; MWI Veterinary Supply), and xylazine (20mg/kg; MWI Veterinary Supply). Mice were transcardially perfused with ice cold PBS and tissue was dissected and submerged in Tri Reagent (Zymo Research). Alternatively, oligodendrocyte lineage cells were sorted from whole tissue as described above. RNA was isolated using either the Direct-zol RNA MicroPrep kit (Zymo Research) (for cells) or by conventional chloroform-isopropanol-ethanol extraction methods (for tissue). For the latter, tissue in Tri Reagent is diluted in chloroform in a 5:1 Tri Reagent:chloroform ratio. After centrifugation at 12000rpm, the clear upper phase is collected and ice-cold isopropanol is added. After 12 minutes centrifugation at 12000rpm, 75% ethanol is added to the pellet. After subsequent centrifugation (12000rpm, 10 minutes), the RNA pellet is dried and dissolved in purified water. RNA concentration was measured by nanodrop (ThermoScientific). RNA then underwent reverse transcription into cDNA using the High Capacity cDNA reverse transcription kit (Thermo Scientific). To detect relative gene expression, inventoried assay Taqman probes targeting *Mct1, Mct2, Mct4, Cx43, Cx30, Cx47, Glut1*, *Glut3* and *Gapdh* (endogenous control) were used throughout the manuscript (for details see Key Resources Table).

Electron microscopy

Mice were deeply anesthetized by I.P. injections of anesthetic cocktail acepromazine maleate (3mg/kg; MWI Veterinary Supply), ketamine (100mg/kg; MWI Veterinary Supply), and xylazine (20mg/kg; MWI Veterinary Supply). Mice were subsequently transcardially perfused with 0.1M Sorensen's phosphate buffer to flush out the blood and subsequently perfused with 4% paraformaldehyde/2.5% glutaraldehyde in 0.1M phosphate buffer. Optic nerves were dissected and post-fixed with 2% osmium for 2 hours. The tissue was subsequently dehydrated in graded ethanol and embedded in Embed 812 resin (EMS). Thin sections (70-80nm) were cut on a Reichert Jung Ultracut E microtome and placed on formvar coated 100 mesh copper grids. The sections were stained with uranyl acetate followed by lead citrate. All imaging was performed on a Zeiss Libra 120 with a Veleta (Olympus) camera at an accelerating voltage of 120Kv. For light microscopy, 0.5μm sections were cut and stained with 1% toluidine blue (EMS).

Lactate and pyruvate transport assay

Lactate and pyruvate transport assays were performed on oligodendrocyte progenitor cell cultures. After culturing oligodendrocytes and plating, oligodendrocyte progenitors were grown for 3 days in oligodendrocyte before lactate/pyruvate transport in oligodendrocyte lineage cells was measured with the lactate/pyruvate transport assay.

For measuring lactate/pyruvate uptake, cells underwent two rounds of washing in HEBSS buffer (25mM HEPES, 150mM NaCl, 3mM KCl, 1.7mM KH_2PO_4, 0.6mM $MgCl_2$ and 1mM $CaCl_2$*$2H_2O$). Cells were then exposed to 2X Hot Lactate/Pyruvate solution (0.5μCi/mL of [^{14}C]-L-lactate/[^{14}C] Pyruvate, PerkinElmer) for 1 min. on ice. The cells treated with MCT1 inhibitor were incubated with 1uM of AR-C1554858 (Tocris) in HEBSS buffer for 10 min. on ice. Cells were washed twice with HEBSS buffer containing 2mM 4-CIN. Cells were incubated in 0.1N NaOH. Plates were swirled to detach the cells from the bottom of the plate and cells were lysed by pipetting cells up and down for 30 times. 500μl of the supernatant is transferred to a scintillation vial and 3 mL of scintillation fluid is added to each sample. Samples are placed on a shaker overnight at room temperature. 200μl of each sample is transferred to a 96 well plate and radioactivity of the samples is measured with scintillation counting machine. The remaining supernatants obtained after cell lysis is used to measure protein concentration using the Bradford assay with the colorimetric reaction measured on a SpectraMax M3 plate reader (Molecular Devices).

Electrophysiological recording

Optic nerve recordings were performed on P360 Sox10^{Cre}-MCT1^{lox} mice and MCT1^{lox} controls as described previously (Larson et al., 2018). Mice were anaesthetized with isoflurane and sacrificed by cervical dislocation. Optic nerves were then rapidly dissected and incubated at room temperature in oxygenated ACSF for $\geq$ 30 min. Nerves were then transferred to a recording chamber superfused with oxygenated ACSF at 37°C (temperature controller, Cell MicroControls TC2BIP 2/3Ch). Using gentle suction, each end of the nerve was drawn into the tip of a flared pipette electrode. The stimulating electrode (containing the retinal end of the nerve) was connected to a constant current isolated stimulator unit (Winston Electronics Co., St. Louis, MO) driven by pClamp9 software (Molecular Devices). CAPs were elicited by a 1 mA, 50 μs current pulse. The recording electrode (containing the chiasmatic end of the nerve) was connected to one input channel of a Multiclamp 700A amplifier (Axon Instruments). A second electrode, placed near the recording electrode but not in contact with the nerve, was connected to the second channel of the amplifier, and the two signals were subtracted on-line by routing through a differential amplifier (Model 440, Brownlee Precision), significantly reducing the stimulus artifact. Signals were filtered at 1 kHz, digitized at 100 kHz using a Digidata 1322A digitizer (Axon Instruments), and recorded to disk using pClamp9 software (Molecular Devices). Data were analyzed offline using MATLAB custom scripts.

QUANTIFICATION AND STATISTICAL ANALYSIS

Image and data analysis

Images were analyzed using Image-J bundled with Java 1.8.0_112 and Zen 2.3 Lite software. For immunofluorescence, at least 2-15 sections per mouse were analyzed and quantified using Zen 2.3 Lite or Image-J. Cells were quantified within a defined area

as # cells/μm^2. On the electron microscopy images g-ratio's and axonal degenerative phenotypes were measured on > 500 axons per sample from 3-10 images taken at 10000x magnification. Images were taken from a minimum of 5 randomly chosen areas of an optic nerve cross section. Inner and outer area of axons were measured with ImageJ from which the outer and inner axonal diameter was calculated respectively. Axons were scored as degenerated if they were either swollen, had accumulation of intracellular material (vesicles, swollen mitochondria) or dark cytoplasm, or if axons had disappeared altogether with accumulation of redundant myelin loops. Mitochondrial area was calculated with ImageJ bundled with Java 1.8.0_112. For the electrophysiological recordings, data were analyzed using Clampfit 11 (Molecular Devices) and MATLAB (Mathworks). Data collected from each optic nerve was considered a biological replicate.

Statistics

All data throughout the manuscript is represented as mean ± SEM as indicated in the figure legends. All statistical details of the experiments can be found in either the Figure legends or the Supplemental Figure legends including the value of n, the p value and statistical test being used. The p value was considered significant when $p < 0.05$. No subjects were excluded from the datasets in any of the experiments. All data met assumptions for the statistical approach, eg equal variance among groups. All statistical analysis has been performed using GraphPad Prism7.

Cell Reports, Volume *34*

Supplemental Information

MCT1 Deletion in Oligodendrocyte Lineage Cells Causes Late-Onset Hypomyelination and Axonal Degeneration

Thomas Philips, Yevgeniya A. Mironova, Yan Jouroukhin, Jeannie Chew, Svetlana Vidensky, Mohamed H. Farah, Mikhail V. Pletnikov, Dwight E. Bergles, Brett M. Morrison, and Jeffrey D. Rothstein

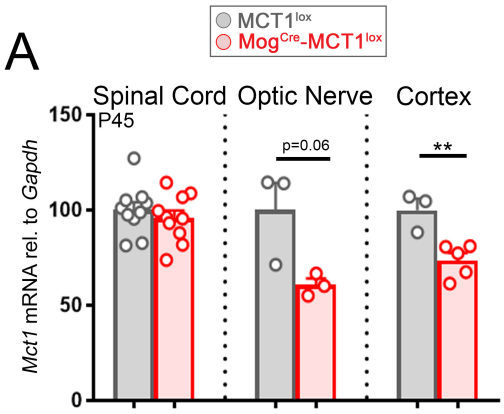
A
MCT1lox
MogCre-MCT1lox
Spinal Cord
Optic Nerve
Cortex
P45
p=0.06
**
Mct1 mRNA rel. to Gapdh
150
100
50
0

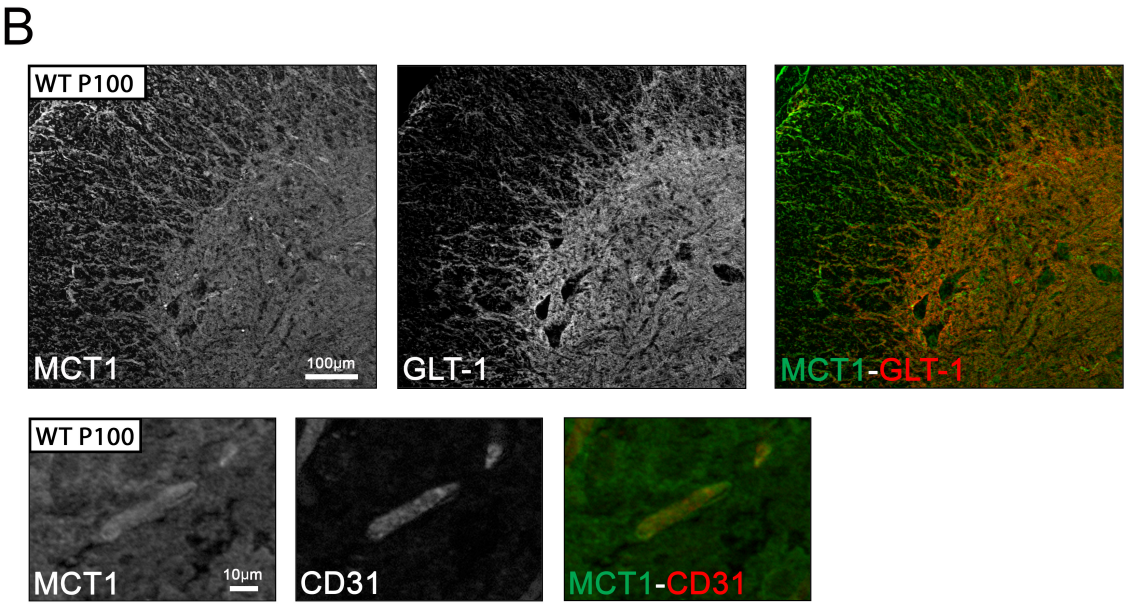
B
WT P100
MCT1
100µm
GLT-1
MCT1-GLT-1
WT P100
MCT1
10µm
CD31
MCT1-CD31

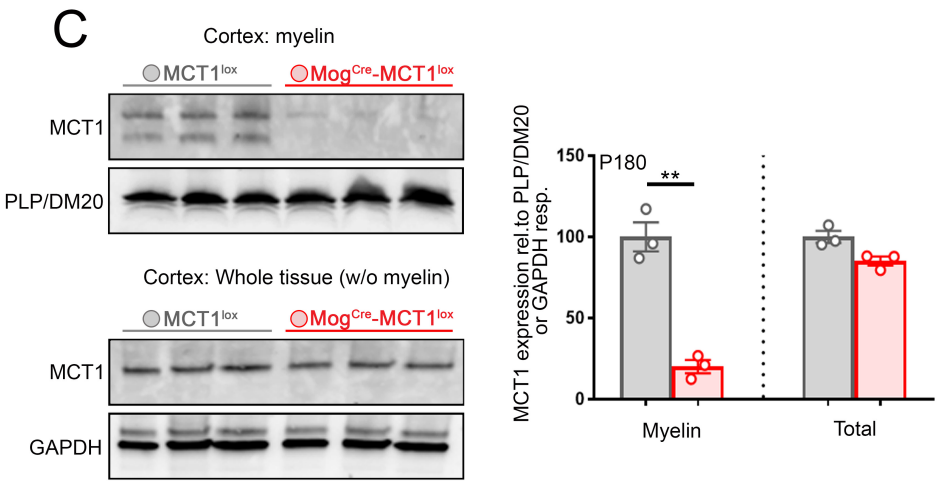
C
Cortex: myelin
MCT1lox
MogCre-MCT1lox
MCT1
PLP/DM20
Cortex: Whole tissue (w/o myelin)
MCT1lox
MogCre-MCT1lox
MCT1
GAPDH
MCT1 expression rel.to PLP/DM20 or GAPDH resp.
P180
**
150
100
50
0
Myelin
Total

Figure S1: Validation of mRNA and protein changes in the Mog^{Cre}-$MCT1^{lox}$ mice and $MCT1^{lox}$ mice and MCT1 antibody immunostaining validation in astrocytes and endothelial cells. Related to Figure 2.

(A) Quantification of *Mct1* mRNA in P45 Mog^{Cre}-$MCT1^{lox}$ and $MCT1^{lox}$ mice in different CNS regions. There is a 26% reduction in *Mct1* mRNA in whole cortex RNA extracts (n=3-10, **p<0.01, Student's t-test). Data is represented as mean ± SEM.

(B) Top panel: Co-Immunolabeling of MCT1 and GLT-1 in astrocytes in the mouse lumbar spinal cord of P100 non-transgenic animals (WT). Bottom panel: Co-immunolabeling of MCT1 and CD31 in endothelial cells in the mouse lumbar spinal cord of P100 non-transgenic animals (WT).

(C) Quantification of MCT1 protein in myelin protein extracts derived from P180 Mog^{Cre}-$MCT1^{lox}$ and $MCT1^{lox}$ cortical tissue. There is an 80% reduction in myelin MCT1 protein expression (n=3, **p<0.01, Student's t-test). Expression in whole tissue (without myelin) was not different between Mog^{Cre}-$MCT1^{lox}$ and $MCT1^{lox}$ mice. Data is represented as mean ± SEM.

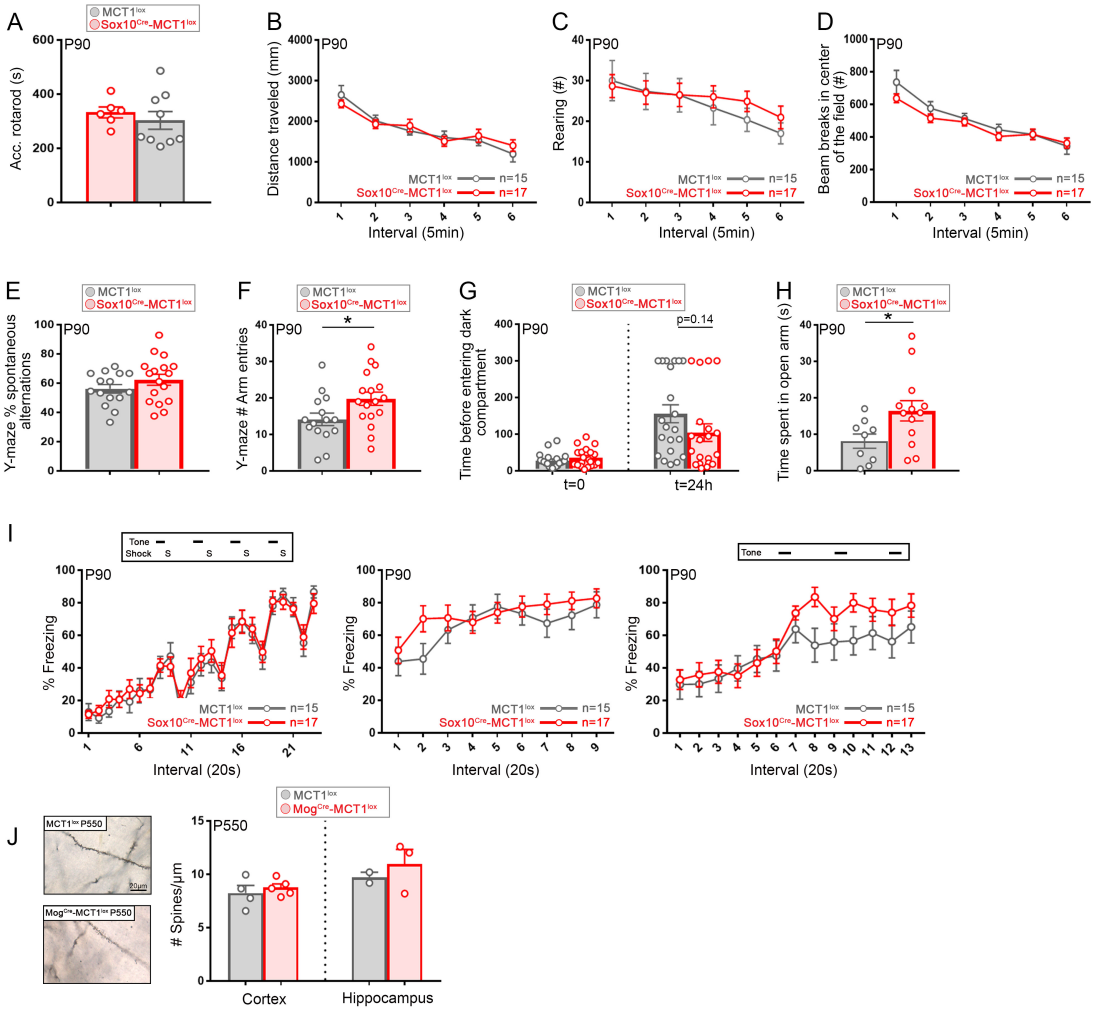

Figure S2: Behavior analysis of P90 Sox10^{Cre}-MCT1^{lox} and MCT1^{lox} littermates control mice. Related to Figure 4.

(A) Accelerated rotarod test does not reveal significant differences between Sox10^{Cre}-MCT1^{lox} and MCT1^{lox} littermates (n=6-9). Data is represented as mean ± SEM.

(B-D) Open field testing does not show any differences in distance travelled (B), rearing (C) and presence in the center versus periphery (D) between $Sox10^{Cre}$-$MCT1^{lox}$ and $MCT1^{lox}$ littermates (n=15-17). Data is represented as mean ± SEM.

(E-F) Working memory assessment in Y-maze does not reveal differences in % spontaneous alternations but showed a 1.4-fold increase in the number of arm entries in the $Sox10^{Cre}$-$MCT1^{lox}$ mice as compared to the $MCT1^{lox}$ controls (n=15-17, *p<0.05, Student's t-test). Data is represented as mean ± SEM.

(G) Passive avoidance test does not reveal differences between $Sox10^{Cre}$-$MCT1^{lox}$ and $MCT1^{lox}$ mice. t=0: the delay for entering a dark compartment after being placed in a brightly lit compartment. The mouse undergoes a 0.5mV shock when entering the dark compartment. t=24h: the delay for each mouse to enter the dark compartment 24 hours after it has been shocked (n=20-21). Data is represented as mean ± SEM.

(H) Time spent in the open arm of the Elevated Plus Maze. There is a 2-fold increase in the percentage of time spent in the open arm in the $Sox10^{Cre}$-$MCT1^{lox}$ as compared to the $MCT1^{lox}$ controls (n=9-13, *p<0.05, Student's t-test). Data is represented as mean ± SEM.

(I) Fear trace conditioning test. Left panel: Training stage: Freezing behavior 24 hours after being preconditioned in the same environment. Mice were exposed to a 90dB tone for 20 seconds for 4 consecutive times. All 4 tones were followed by a 0.5 mV shock for 2 seconds. Middle panel: Context phase: Freezing behavior in the same environment as where the mouse was shocked 24 hours earlier. Right panel: Cued phase: Freezing behavior after hearing 3 bouts of the same tone as in the training phase. The mouse has been placed in a different environment as compared to the earlier phases. There

are no significant differences in freezing behavior at any stage between the Sox10^{Cre}-MCT1^{lox} and MCT1^{lox} mice (n=15-17). Data is represented as mean ± SEM.

(J) Spine density measurements in the cortex and hippocampus of P550 Mog^{Cre}-MCT1^{lox} and MCT1^{lox} littermate controls reveal no significant differences (n=2-5). Data is represented as mean ± SEM.

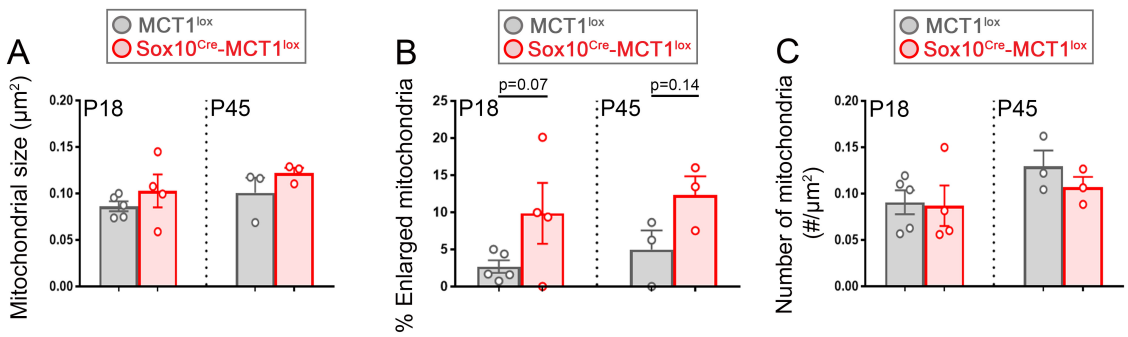
A
MCT1lox
Sox10Cre-MCT1lox
Mitochondrial size (µm²)
P18
P45
B
% Enlarged mitochondria
p=0.07
p=0.14
C
Number of mitochondria (#/µm²)

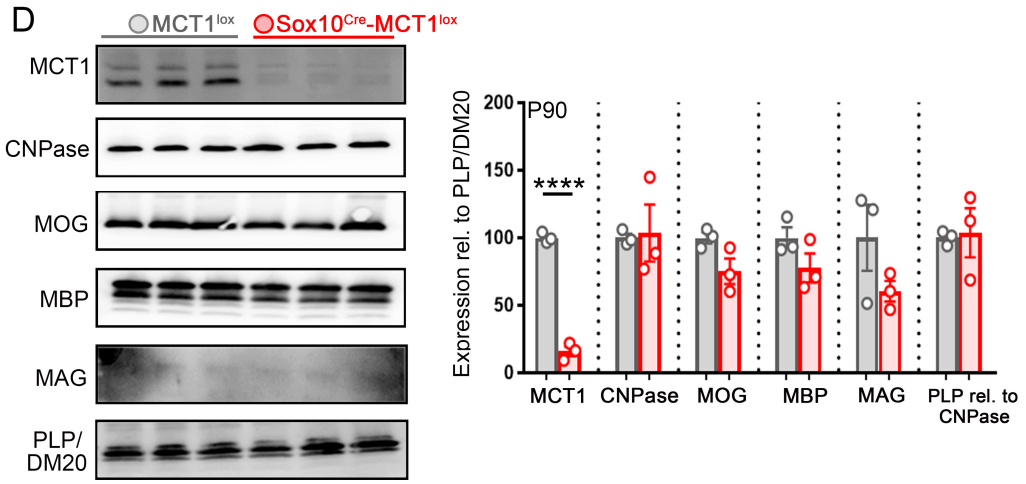
D
MCT1lox
Sox10Cre-MCT1lox
MCT1
CNPase
MOG
MBP
MAG
PLP/
DM20
P90
****
Expression rel. to PLP/DM20
MCT1
CNPase
MOG
MBP
MAG
PLP rel. to CNPase

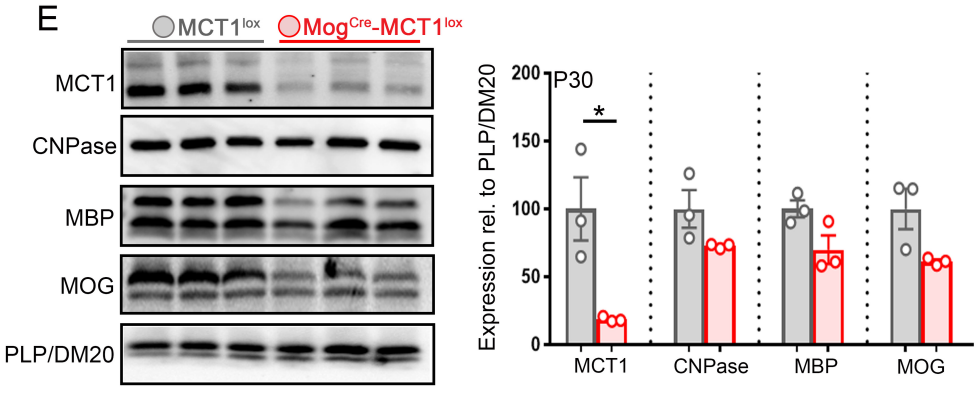
E
MCT1lox
MogCre-MCT1lox
MCT1
CNPase
MBP
MOG
PLP/DM20
P30
*
Expression rel. to PLP/DM20
MCT1
CNPase
MBP
MOG

Figure S3: Analysis of mitochondrial size in P18 and P45 Sox10^{Cre}-MCT1^{lox} mice and myelin protein expression in early adult Sox10^{Cre}-MCT1^{lox}, Mog^{Cre}-MCT1^{lox} mice compared to MCT1^{lox} mice. Related to Figure 4.

(A-B) Analysis of electron microscopic images of optic nerve axons indicates there is no difference in mitochondrial size (A) or % of enlarged mitochondria (>0.20um^2, B) between Sox10^{Cre}-MCT1^{lox} and MCT1^{lox} mice at either P18 or P45 (n=3-5). Data is represented as mean ± SEM.

(C) Analysis of electron microscopic images of optic nerve axons indicates there is no difference in the number of mitochondria when comparing Sox10^{Cre}-MCT1^{lox} and MCT1^{lox} mice at either P18 or P45 (n=4-5). Data is represented as mean ± SEM.

(D) Changes in expression of myelin proteins in cortical myelin protein extracts derived from P90 Sox10^{Cre}-MCT1^{lox} and MCT1^{lox} control mice. There is an 84% reduction in expression of MCT1 whereas expression of CNPase, MBP, MOG and MAG was unchanged as compared to MCT1^{lox} controls (n=3, ****p<0.0001, Student's t-test). Data is represented as mean ± SEM.

(E) Changes in expression of myelin proteins in spinal cord myelin protein extracts derived from P30 Mog^{Cre}-MCT1^{lox} and MCT1^{lox} control mice. There is an 81% reduction in expression of MCT1 while the expression of MOG, CNPase and MBP was unchanged as compared to MCT1^{lox} controls (n=3, *p<0.05, Student's t-test). Data is represented as mean ± SEM.

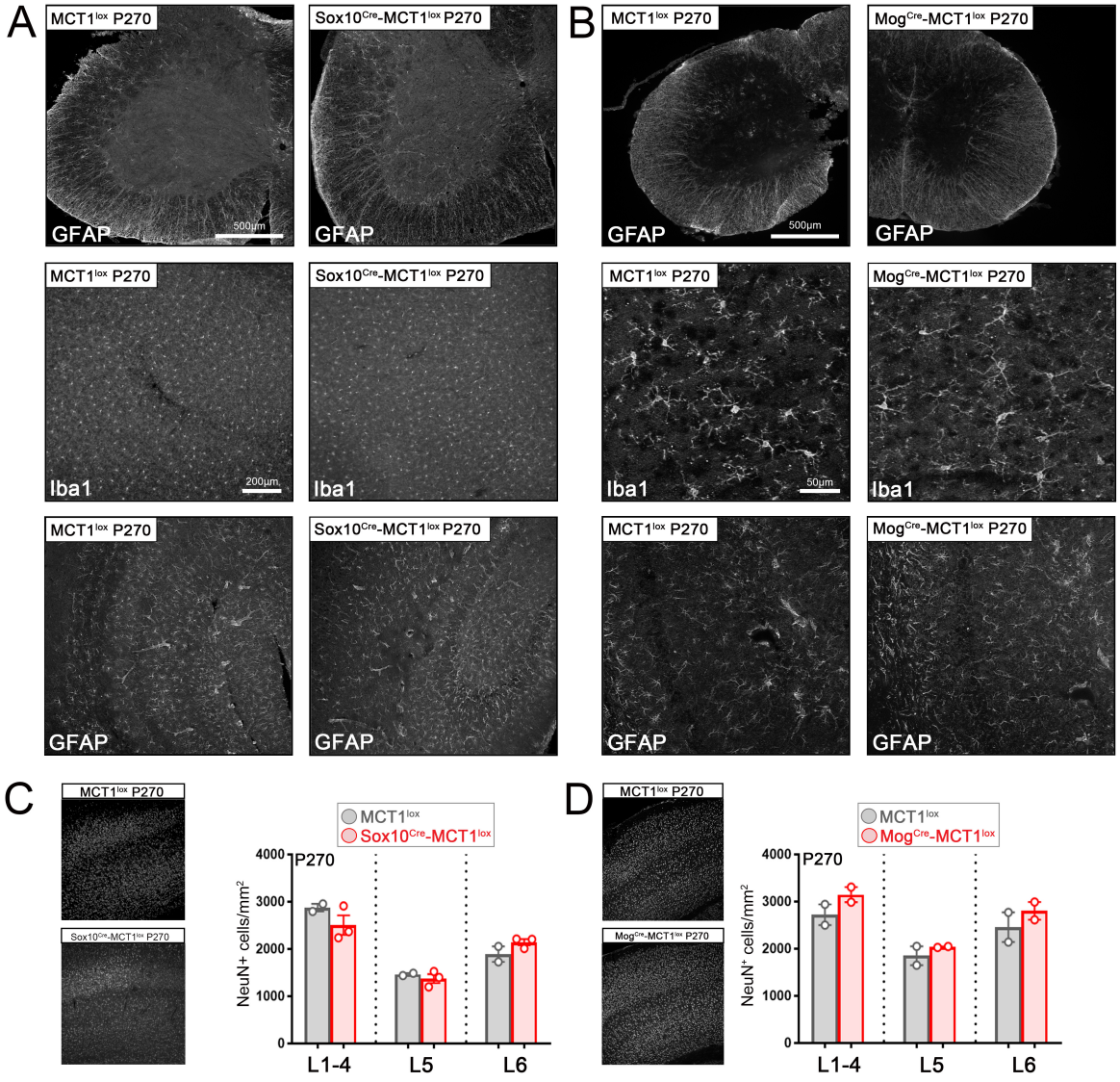

Figure S4: Glial reactivity and neuronal cell density measurements in spinal cord, cortex and hippocampus of P270 Sox10^{Cre}-MCT1^{lox}, Mog^{Cre}-MCT1^{lox} and MCT1^{lox} mice. Related to Figure 5 and Figure 6.

(A) GFAP and Iba1 immunostaining in the lumbar spinal cord (top panel), cortex (middle panel) and hippocampus (lower panel) does not reveal changes in glial reactivity when comparing P270 $Sox10^{Cre}$-$MCT1^{lox}$ and $MCT1^{lox}$ controls.

(B) GFAP and Iba1 immunostaining in the cervical spinal cord (top panel), cortex (middle panel) and hippocampus (lower panel) does not reveal changes in glial reactivity when comparing P270 Mog^{Cre}-$MCT1^{lox}$ and $MCT1^{lox}$ controls.

(C) There is no difference in the number of $NeuN^{+}$ neurons quantified in the cortex layer 1-4 (L4), layer 5 (L5) and layer 6 (L6) in P270 $Sox10^{Cre}$-$MCT1^{lox}$ and $MCT1^{lox}$ controls (n=2-3). Data is represented as mean ± SEM.

(D) There is no difference in the number of $NeuN^{+}$ neurons quantified in the cortex layer 1-4 (L4), layer 5 (L5) and layer 6 (L6) in P270 Mog^{Cre}-$MCT1^{lox}$ and $MCT1^{lox}$ controls (n=2). Data is represented as mean ± SEM.

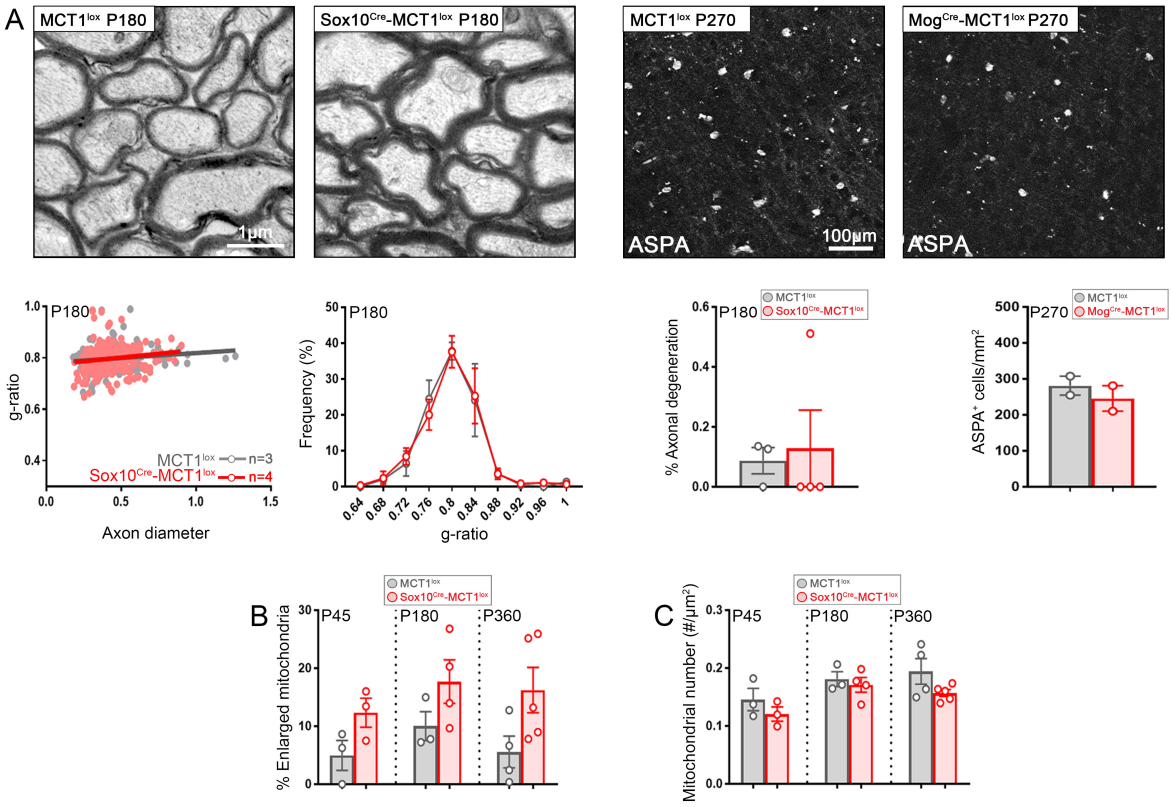

Figure S5: Evaluation of myelin thickness, oligodendrocyte cell counts and mitochondrial size in P45-P360 Sox10^{Cre}-MCT1^{lox}, Mog^{Cre}-MCT1^{lox} and MCT1^{lox} mice. Related to Figure 5 and Figure 6.

(A) Left panels: Electron microscopy images from the optic nerves form P180 Sox10^{Cre}-MCT1^{lox} and MCT1^{lox} controls. There is no axonal pathology and no change in myelin thickness (g-ratio) is observed (n=3-4). Right panels: Immunostaining of ASPA^{+} oligodendrocytes counted in the cortex of P270 Mog^{Cre}-MCT1^{lox} and MCT1^{lox} controls. The number of oligodendrocytes was not different between the two groups (n=2). Data is represented as mean ± SEM.

(B) There are no differences in the percentage of enlarged mitochondria (>0.20µm^2) as observed on electron microscopy images taken from optic nerves dissected from P45, P180 and P360 old Sox10^{Cre}-MCT1^{lox} and MCT1^{lox} mice (n=3-5). Data is represented as mean ± SEM.

(C) There are no differences in the number of mitochondria (per μm^2) measured on electron microscopy images taken from optic nerves dissected from P45, P180 and P360 old $Sox10^{Cre}$-$MCT1^{lox}$ and $MCT1^{lox}$ mice (n=3-5). Data is represented as mean ± SEM.

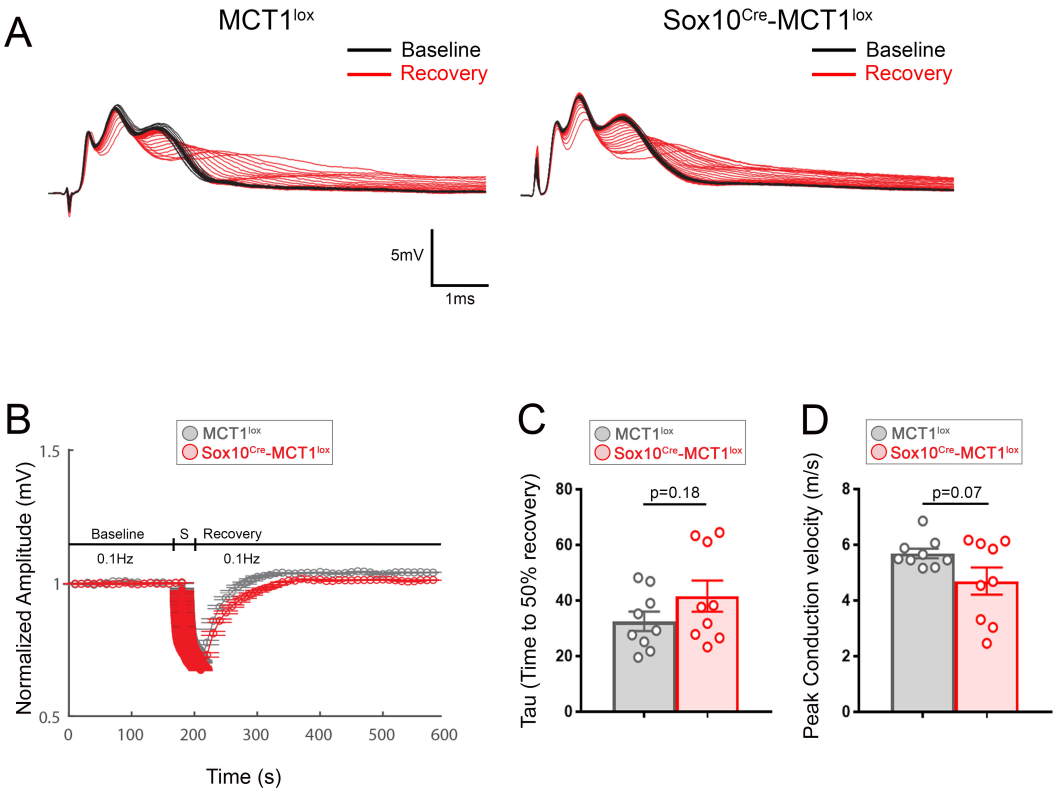

Figure S6: Optic nerve electrophysiological recordings from P360 Sox10^{Cre}-MCT1^{lox} and MCT1^{lox} optic nerves. Related to Figure 6.

(A) Electrophysiological recording traces at baseline (black line) and during recovery (red line) in optic nerves isolated from either P360 MCT1^{lox} (left panel) or P360 Sox10^{Cre}-MCT1^{lox} (right panel) mice (n=9).

(B) Normalized peak amplitude at baseline (0.1Hz stimulation), during a 30 sec. high frequency stimulation (100Hz) (S) and during 5 min. recovery (0.1Hz) in P360 MCT1^{lox} and Sox10^{Cre}-MCT1^{lox} optic nerves. No significant differences are recorded between the two groups (n=9).

(C) There is no significant difference between P360 MCT1^{lox} and Sox10^{Cre}-MCT1^{lox} optic nerves for Tau recovery time (50% recovery) after a high frequency stimulation burst (n=9). Data is represented as mean ± SEM.

(D) There is no significant difference between P360 MCT1^{lox} and Sox10^{Cre}-MCT1^{lox} optic nerves for peak conduction velocity after electrophysiological stimulation (n=9). Data is represented as mean ± SEM.

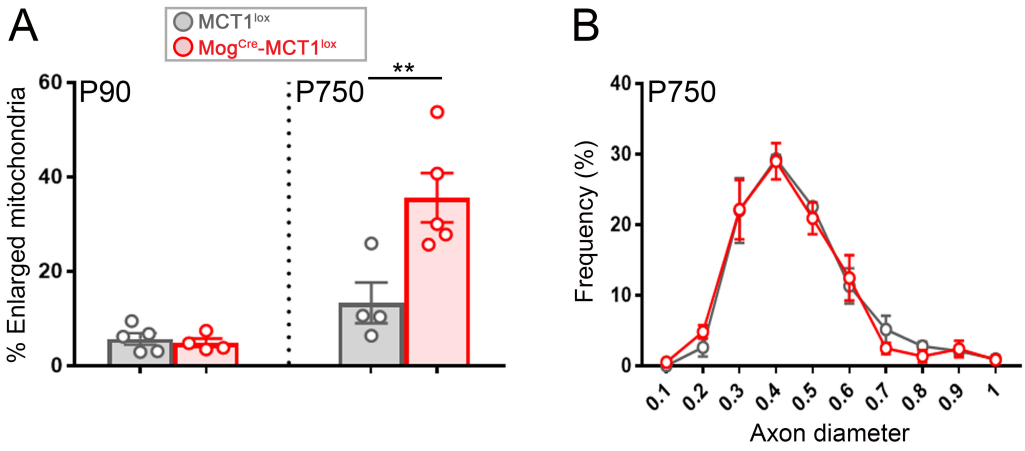

Figure S7: Mitochondrial size and axon size distribution in P750 Mog^{Cre}-MCT1^{lox} and MCT1^{lox} mice. Related to Figure 7.

(A) The percentage of enlarged mitochondria was unchanged in P90 Mog^{Cre}-MCT1^{lox} but increased 2.7-fold in P750 optic nerves dissected from Mog^{Cre}-MCT1^{lox} and MCT1^{lox} controls (n=4-5, **p<0.01, two-way ANOVA with Sidak's multi-comparison test). Data is represented as mean ± SEM.

(B) There is no change in axon size distribution between P750 Mog^{Cre}-MCT1^{lox} and MCT1^{lox} controls (n=4-5). Data is represented as mean ± SEM.

Study	Output	n	Results
Accelerated Rotarod	Motor performance	6-9	n.s. p=0.51
Open Field	General locomotor Activity - Distance traveled - Speed - Rearing - Cen vs Per	15-17	 n.s. p=0.96 n.s. p=0.63 n.s. p=0.69 n.s. p=0.42
Catwalk	Gait, balance, stride - Stride length	6-9	 n.s. p=0.32
Elevated Plus Maze	Anxiety	9-13	*p<0.05
Y maze spontaneous alternations	Working memory - Spontaneous alternations - Arm entries	15-17	 n.s. p=0.21 *p<0.05
Passive avoidance test	Learning/memory (fear)	20-21	n.s. p=0.14
Fear Trace conditioning	Learning/memory (fear) - Context - Cued	15-17	 n.s. p=0.76 n.s. p=0.68

Table S1: Overview of the different animal behavior studies performed on P90 Sox10^{Cre}-MCT1^{lox} and MCT1^{lox} mice. Related to Supplemental Figure 2.

Mct1 het mice	Sox10^{Cre}-MCT1^{lox} mice	Mog^{Cre}-MCT1^{lox} mice
Optic nerve axonopathy by P240	Axonal degeneration by P360	No axonal degeneration by P360 Prominent axonal degeneration by P750
Enhanced glial reactivity by P240 in cortex and hippocampus	Enhanced microglial reactivity by P360, no change in astrocyte reactivity	No changes in glial reactivity up to P270
No myelin deficiencies by P240	Hypomyelination by P360	No myelin deficiencies

Table S2: Side by side comparison of observed phenotypes in *Mct1* het mice, Sox10^{Cre}-MCT1^{lox} mice and Mog^{Cre}-MCT1^{lox} mice. Related to Figures 5-7.